11 Trigger performance

11.1 Introduction

This chapter presents a summary of the ATLAS level-1 (LVL1) and level-2 (LVL2) triggers and outlines the task of the Event Filter (EF). Details of the algorithms and justification of the proposed selections are explained in [11-1]. Technical details of the LVL1 muon and calorimeter trigger implementation are documented in [11-2]. This chapter is restricted to the presently accepted algorithms, their key selections and resulting efficiencies and rates.

Section 11.2 presents an overview of the ATLAS trigger strategy and summarises the functionality. The next sections present the trigger algorithms and their performance. Section 11.3 is devoted to the LVL1 trigger: the muon trigger and various calorimeter triggers. The trigger objects selected by LVL1 constitute the input to the higher-level triggers, LVL2 and EF. The RoI-guided triggers are summarised in Section 11.4, followed by triggers that do not need RoI guidance, missing-transverse energy (Section 11.5) and the *B*–physics trigger channels (Section 11.6). The resulting sets of trigger objects are input to the global LVL1 and LVL2 decisions, which are driven by lists of hypotheses derived from the list of physics signatures of interest (Section 11.7). The last section presents the task of the Event Filter (Section 11.8).

The present chapter addresses only some of the issues associated with trigger performance. The studies need to be extended and consolidated. The overall optimisation of the trigger implementation, taking into account processing power, data bandwidth and cost requirements, will be a joint task of the LVL2, EF and trigger performance group during the coming years. Especially the work for the EF will need the cooperation of the physics and reconstruction groups to develop the selections and the selection tools.

11.2 Overview of ATLAS trigger strategy

11.2.1 Introduction

The main challenges at the LHC that have an impact on the experiment's trigger system are an unprecedented rate of 10^9 interactions per second, the need to select rare predicted physics processes with high efficiency while rejecting much higher-rate background processes, and large and complex detectors with huge numbers of channels O(10^7). Decisions must be taken every 25 ns; at high luminosity, each bunch crossing contains about 23 interactions. At the end of the decision chain, the event storage rate is limited to approximately 100 Hz, by practical limitations in the offline computing power and storage capacity. The average event size is 1 Mbyte [11-3].

The ATLAS trigger strategy foresees a reduction of the event rate at three levels: LVL1, LVL2 and Event Filter [11-3]. The accepted rates at each level are given in Figure 11-1. The LVL1 trigger receives data at the full LHC bunch-crossing rate of 40 MHz. The output rate is limited by the capabilities of the front-end systems to 75 kHz (upgradable to 100 kHz). The present esti-

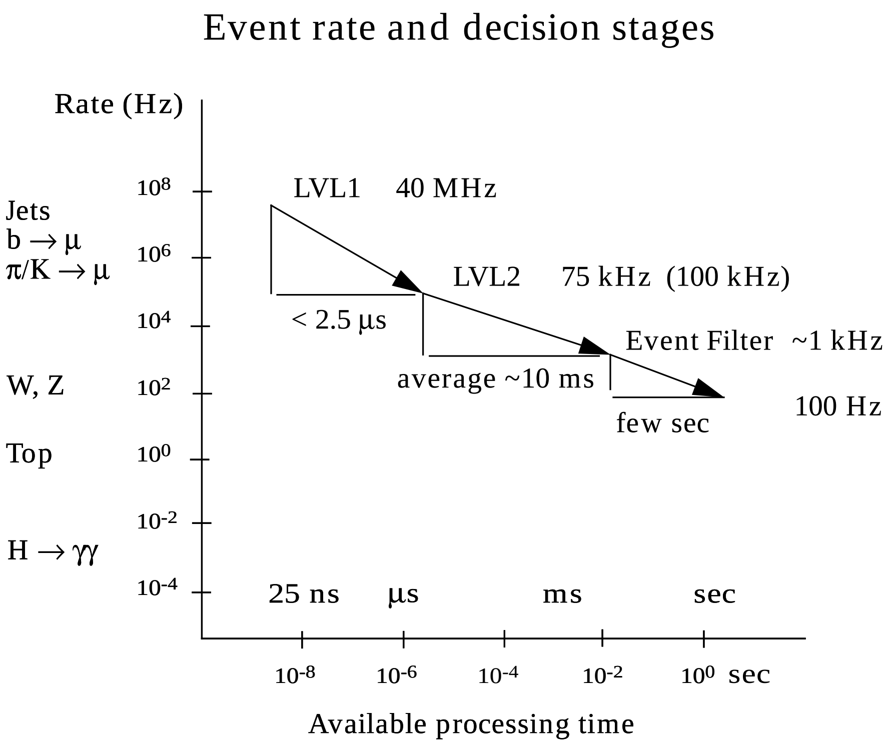

Figure 11-1 The three levels of the ATLAS trigger and their event rates and processing times.

mate of rates, as given in Section 11.7, allows for a safety margin of about a factor of two on the output rate from LVL1. Furthermore, thresholds are deliberately chosen to be lower than strictly necessary for the success of the ATLAS physics programme.

LVL2 and the EF combined will give a reduction factor of order 10^3, where LVL2 is expected to provide a reduction of a factor of about 100 resulting in an input rate to the EF of the order of 1 kHz. The sharing of the selection task between LVL2 and the EF remains to be optimised, so the output rate from the LVL2 trigger is not final. Similarly, there is some flexibility on the output rate from the EF.

The following sections describe the essential steps in the trigger-decision chain and the trigger 'objects' that are used in the selection process. The status and workplan of the LVL2, data acquisition and event filter projects are described in [11-4]. The trigger algorithms at LVL1 must be relatively simple in order to be implemented in very fast custom hardware processors. Much more freedom for algorithm complexity and programmability is available at LVL2 and in the EF. Indeed, both of these high-level triggers may well be implemented using very similar, or even the same, communication and computing structures. They differ only in the way that detector data is accessed and by the framework for software and database access. Simple, fast algorithms are foreseen for LVL2, whereas more offline-like algorithms are applied in the EF. Technology evolution indicates an increase in CPU processing power by an order of magnitude over the next five years and an increase in memory density by a factor of four every two years. A firm division between LVL2 and the EF is therefore premature and even not desirable. The tasks have to be specified, and their physical location, where they are executed, may shift with time. The allocation depends on the evolution of technology and improved understanding of the tasks. This process of optimisation will continue after data taking begins.

11.2.2 LVL1 trigger and regions of interest

The LVL1 trigger [11-2] identifies the basic signatures of ‘interesting’ physics with high efficiency. It forms its decision on the basis of multiplicities for the following local trigger objects for various p_T thresholds: muon, EM clusters (where isolation can be required), narrow jets (isolated hadronic τ decays or isolated single hadrons), jets and the global objects: missing transverse energy, total scalar transverse energy.

The muon and calorimeter LVL1 trigger systems use simple algorithms to make fast decisions. Local pattern recognition and transverse-energy evaluation are performed on prompt, relatively coarse-grained information, which is provided by the fast muon trigger chambers and the tower summing electronics of the EM and hadronic Calorimeters.

The LVL1 algorithms are executed by custom electronics, programmed in terms of adjustable parameters. The decision time of ~2 μs includes the transmission of signals between the detector and the trigger electronics. During the LVL1 trigger processing, the data from all detector systems are held in pipeline memories. When LVL1 has accepted an event, the data are read out, formatted and initial preprocessing may be applied (*e.g.* calibration) before they are stored in readout buffers (ROBs) for use by the LVL2 trigger and the EF.

The LVL2 trigger is largely based on the use of regions of interest (RoIs). For each event accepted by LVL1, a small amount of information is passed to LVL2 corresponding to each object identified at LVL1. For local objects, such as muons and EM clusters, the information provided is position (η, ϕ) and p_T threshold range. These RoIs flag the regions that need to be analysed further by higher-level triggers. Also provided by LVL1 are the components of the missing-E_T vector and the total scalar E_T value, as well as information on the criteria that led to the event being selected.

LVL2 processors perform local evaluation of the objects identified at LVL1 using the fine-grained detector data in a window around the position indicated by the RoI. Thus, usually only a small fraction of the event data need to be moved from the ROBs to the designated processor, thereby reducing the required bandwidth and processing power at LVL2.

11.2.3 LVL2 data collection and feature extraction

At LVL2 each RoI is examined in the detector system from which it originated, *i.e.* in the muon or calorimeter system, to see if it is confirmed as a valid object. After the confirmation of the LVL1 RoI, additional features associated with it may be searched for in other detectors, such as the SCT / Pixel and TRT. This is the case for muon, EM cluster and τ RoIs. Jet RoIs are only processed in the calorimeters, with the possible exception of *b*-jet tagging, which requires tracking detectors to evaluate the impact parameters of tracks.

The information from all systems is then combined to form more specialised global trigger objects, which become candidates for muons, electrons, photons, τ's, and jets, as well as generalised missing-E_T and B-physics objects. These LVL2 global objects form the input to the LVL2 global decision. An average processing time of ~10 ms per event is currently assumed for the LVL2 trigger.

Processing of B-hadron events is different from standard RoI processing. B-hadron events are triggered by a low-p_T single muon at LVL1. This muon is then confirmed at LVL2 in the muon spectrometer and the Inner Detector. For events retained after this initial selection, a full track search must then be performed to allow decisions based on semi-exclusive B-event hypotheses. The present strategy is to search for tracks in the TRT with very low p_T thresholds. The resulting TRT tracks are used to define additional RoIs (so-called LVL2 RoIs) that guide further track searches in the SCT. The reconstructed SCT tracks, giving information in three dimensions, allow for the calculation of invariant masses; they may be extrapolated into the calorimeter or Muon Systems to confirm low-p_T lepton candidates, in conjunction with the transition–radiation signature from the TRT in the case of electrons.

The RoI information from LVL1 gives the position of the object with a typical resolution ranging from about $\Delta\eta\times\Delta\phi = 0.1\times0.1$ (leptons and photons) to about 0.4×0.4 (jets) in pseudorapidity–azimuthal angle space. The area over which the LVL2 algorithms require data is generally larger than this and has to be adapted to the detector system in question and to the algorithms applied at LVL2. For example, for validation of EM clusters in the calorimeters a region of at least about 0.3×0.3 is needed.

11.2.4 Event Filter

The final online selection step is performed by the EF. Here the full event is collected from the different data sources (ROBs) and the EF operates on the complete event using the full-granularity of the detector. The processing time is of the order of seconds. A refined reconstruction is possible using offline-like algorithms, though calibration and alignment constants are not the final ones. Vertex reconstruction and track fitting, including bremsstrahlung recovery for electrons, are examples of algorithms that could be executed at this level. Other examples are operations that require larger RoIs than those used at LVL2, such as γ conversion searches or calculations requiring the complete event data, as is the case for missing E_T. The LVL1 and LVL2 results will guide the EF processing chain, in a mode that is similar to the guidance of LVL2 by LVL1 RoIs. The EF completes the classification of the events, establishes a catalogue of discovery-type events ('express line'), and stores accepted events in the database. Events may be directed to separate output streams, for example if they are needed for calibration or alignment purposes only. Details of the EF are described in [11-4].

11.2.5 Trigger objects and the trigger-decision chain

11.2.5.1 Trigger objects

Through the selection chain from LVL1 to the EF, the trigger objects are progressively refined and made more specific. New trigger objects may be added at LVL2 and in the EF. Trigger objects are combined in 'physics menus': lists of selection criteria which will be described in more detail in Section 11.7. The following sections introduce the essential features of the objects and describe the global decisions at LVL1 and LVL2. Detailed selection criteria at the level of individual objects are presented in [11-1] and are summarised in Sections 11.3.1 and 11.3.2 for the LVL1 trigger, and in Sections 11.4 to 11.6 for the LVL2 triggers.

LVL1 objects are characterised by a small number of attributes and a set of discrete p_T-threshold values. They are listed in Table 11-1 together with the corresponding pseudorapidity coverage. The number of thresholds is six for the muon trigger; sixteen thresholds are shared between the EM cluster and τ/hadron calorimeter triggers, eight thresholds are used for the E_T^{miss} trigger and four for the total scalar E_T trigger. More precisely, the 'thresholds' of the EM cluster trigger and the τ/ hadron trigger each consist of a triplet of thresholds – cluster E_T threshold, and two isolation thresholds for EM and for hadronic E_T depositions. The isolation requirement is relaxed with increasing E_T or for two-cluster triggers; no isolation requirement is made for the highest EM E_T threshold.

LVL1 trigger selections are normally independent of the pseudorapidity, though simple topological requirements can be imposed. For example, jets that pass a given threshold may be required to be produced at central pseudorapidities. A trigger selecting large energy deposition in the forward regions ($|\eta| > 3.2$) is under consideration.

The LVL1 trigger ensures that trigger objects of the same type are not double counted. Overlaps between different trigger categories, however, are not resolved at LVL1. For example, an energetic electron may pass simultaneously as an EM cluster, a τ and a jet trigger. Two muons, if unbalanced in E_T, may give a missing-E_T trigger. Such redundancies are useful for monitoring the trigger. The overlaps are taken into account in the global decision at LVL2. No communication between the systems is available at LVL1. Thus for example, isolation cannot be required for muons.

In addition to the trigger RoIs, LVL1 may indicate other RoIs, typically at lower thresholds. These so-called secondary RoIs do not contribute to the trigger decision at LVL1. They are provided for possible analysis at LVL2 or in the EF and may contribute to the classification of an event.

Table 11-1 LVL1 objects and their attributes in addition to E_T. Tables 11-1 and 11-2 introduce the mnemonics for trigger objects used in the trigger menus, see Section 11.7. A total of 16 thresholds is available for EM and T objects combined.

Object	Number of thresholds	Isolation	$\|\eta\|$ range	description
MU	6	no	2.4	muon
EM	8 – 16	yes	2.5	EM cluster
T	0 – 8	yes	2.5	$\tau \rightarrow$ hadrons or single hadron
J	8	no	3.2	jet
XE	8	–	4.9	missing-E_T
SE	4	–	4.9	total scalar E_T

LVL2 objects are listed in Table 11-2. Their principal attributes are, as at LVL1, p_T threshold and isolation. The complete list of attributes attached to each trigger object is, however, much richer than at LVL1. For example, the EM cluster is described by its transverse energy in several windows, by its lateral and longitudinal shape and by several parameters that characterise the fine-

Table 11-2 LVL2 objects and attributes in addition to E_T. Additional attributes are discussed in Section 11.4.

Object	Attribute	$\|\eta\|$ range	Candidate for
μ	isolation	2.4	muon
e	isolation	2.5	electron
γ	isolation	2.5	photon
τ	isolation	2.5	$\tau \rightarrow$ hadrons
h	isolation	2.5	single hadron
j	b-tag ($\|\eta\| < 2.5$)	3.2	jet
xE	–	4.9	missing-E_T

grained information in the EM preshower compartment. The local features are combined to form global objects, *e.g.* the calorimeter information is combined with the information from the Inner Detector and the quantities that characterise the quality of matching between track and cluster.

The selection criteria may depend on parameters like pseudorapidity. Hence the fine adjustment of parameters in a multi-dimensional space is necessary to achieve optimal background rejection for the highest signal efficiency. Several varieties of electron candidates may be defined, as motivated by the class of physics processes[1]. In practice, simplicity and ease of monitoring are important criteria, which will limit the choice of algorithms, parameters and selection cuts. In Sections 11.4 to 11.6 the trigger algorithms are discussed together with the set of key selection criteria associated with each of these algorithms.

11.2.5.2 Global LVL1 and LVL2 decision

Trigger menus have been derived from the physics requirements. They classify the signatures such that a combination of trigger objects is sufficient to select events. Thresholds and attributes for the trigger objects are optimised to meet the requirements of high efficiencies and acceptable rates. An initial set of trigger menus for low- and high-luminosity running is presented in Section 11.7. Despite the large variety of physics available at the LHC, a short list of inclusive single and multi-object triggers, as well as a small number of combined triggers, are sufficient to cover the expected physics programme. These menus will evolve during the lifetime of the experiment, with improved understanding of the detector, development of technology and shifting physics interest.

The global decision at LVL1 and LVL2 is made by comparing the list of accepted trigger objects to the trigger menus. At LVL1, where the decision must be taken at a rate of 40 MHz, only a small amount of information can be transmitted to the central trigger processor (CTP), which combines the information from the muon and calorimeter triggers. A total of up to 96 menu items are foreseen for the CTP. The triggers are inclusive, and cover physics and detector monitoring, which must run continuously during physics data-taking.

1. This is similar to the choice of looser criteria for two-object triggers at LVL1.

The LVL2 strategy for confirming trigger objects is still under study [11-4]. Much effort is going into the development of algorithms and selection criteria to define trigger objects. Once these are defined, the final global decision is straightforward (except for processing of secondary RoIs, which is discussed below). At LVL2, in addition to requiring combinations of trigger objects, the menus may include functional decisions such as invariant-mass cuts, p_T-sum cuts, *etc*. Mass cuts are expected to be used for *B*-physics objects, and they could be applied wherever objects of known masses are part of the hypothesis, *e.g.* for leptonic decays of the Z^0.

Two different trigger objects may originate from the same physical object. For example, if a menu item requires an electron and a τ candidate, then both of these trigger objects could originate from the same high-p_T electron. The menus of Section 11.7 do not at present require such combinations and are hence sufficiently simple to ensure that such cases do not occur. For future extensions of the menus it will be necessary to ensure that such cases either add negligible rates or are correctly resolved. Algorithms will be needed to compare categories of objects and decide whether they have the same physical origin.

The use of secondary RoIs complicates the LVL2 decision logic, but may contribute to the classification of the events. These RoIs require an additional pass in the decision chain after the trigger RoIs have been confirmed. More studies are needed on the use of secondary RoIs at LVL2 or possibly by the EF. This issue is linked to the overall optimisation of LVL2 and the EF.

11.2.6 Specialised triggers

In addition to the triggers that are motivated by the physics programme, the same or specialised triggers at lower thresholds are needed to measure the trigger efficiency, and to monitor the detector and trigger performance. These include triggers for alignment and calibration. The requirements of the detector systems for such triggers are presently being assessed. Lower prescaled thresholds are also needed for certain physics studies, *e.g.* QCD.

11.3 LVL1 trigger

This section summarises the performance of the algorithms chosen for triggering at LVL1, and for delivering regions-of-interest to the LVL2 trigger. The choices of the algorithms and the hardware implementations are justified in [11-2].

11.3.1 LVL1 muon trigger

11.3.1.1 Trigger algorithms

The LVL1 muon trigger is based on the measurement of muon trajectories in three different planes (called stations). The trigger is described in detail in [11-2]. Muons are deflected by the magnetic field generated by the toroids; the angle of deflection depends on their momentum and the field integral along their trajectory. Coulomb scattering in the material traversed, and for low-p_T triggers, the energy-loss fluctuation, are also of importance.

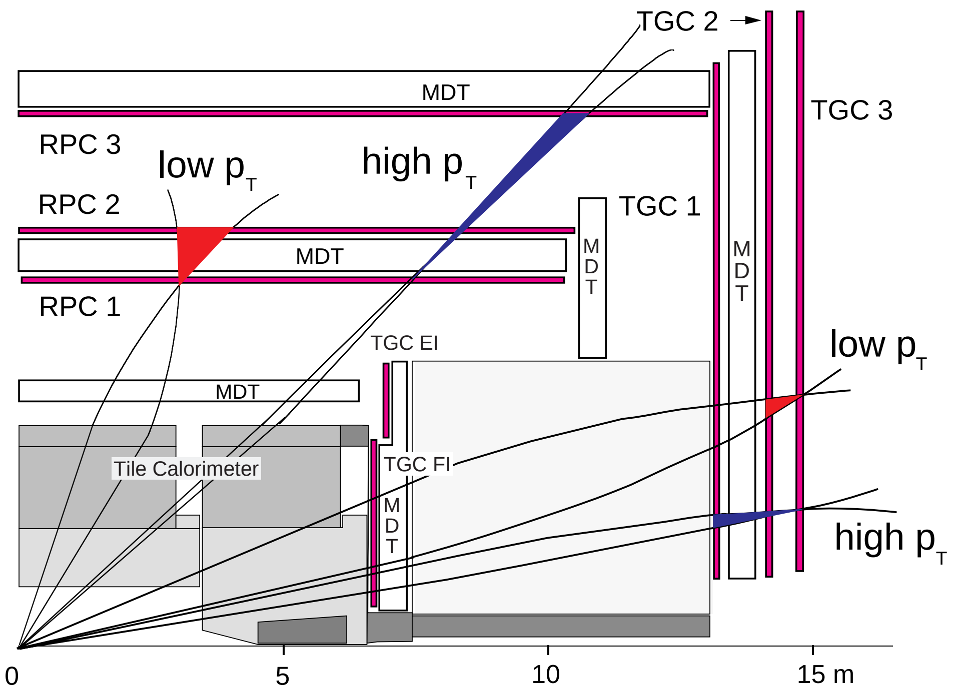

Figure 11-2 The LVL1 muon–trigger scheme.

The differences from a straight-line trajectory of an infinite-momentum track originating at the nominal interaction point are measured using three trigger stations, see Figure 11-2. The trigger plane farthest from the interaction point in the end-cap, and nearest to the interaction point in the barrel, is called the pivot plane. The two different lever arms from the pivot to the other two trigger planes provide two different measurements of the size of the deflection due to the field. The two different lever arms allow trigger thresholds to cover a wide range of transverse momenta with reasonably good resolution: the shorter lever arm (pivot plane and station 2) covers a lower-momentum range and the longer one (pivot plane and station 1 for the end-cap, pivot plane and station 3 for the barrel), a higher-momentum range.

Each hit found in station RPC1 (TGC3) is extrapolated to station RPC2 (TGC2) along a straight line through the nominal interaction point. A coincidence window is then defined around this point, where the window size depends upon the required p_T threshold. The low-p_T trigger condition is then satisfied if, for both projections, there is at least one hit within the coincidence window, and at least one of the two low-p_T stations has hits in both trigger planes satisfying the three-out-of-four logic

A similar procedure is performed for the high-p_T trigger, where the planes of RPC3 (TGC1) together with the pivot plane are used. The high-p_T trigger is satisfied if the track passes the low-p_T criteria, and in the barrel at least one hit in the two trigger planes of RPC3 are in coincidence, and in the end-cap if at least two of the three planes of TGC1 in the η view, and one of the two planes of TGC1 in the r–ϕ view are within the appropriate coincidence window.

The muon-trigger is divided into regions in η–ϕ where independent trigger windows can be used. The size of the coincidence window defines the p_T threshold applied in the trigger – the wider the window, the lower the threshold. Windows are defined such that efficiency at threshold is 90%. A tight time coincidence among hits is also required, to identify the bunch crossing.

11.3.1.2 Options to increase trigger robustness

To increase the flexibility of the trigger to cope with higher backgrounds, and in particular to offer additional robustness against backgrounds from the high flux of charged particles of momentum around 100 MeV (see Section 11.3.1.6), the trigger provides additional coincidence options [11-5].

- In both end-cap and barrel triggers the logic of the high-p_T trigger can be adopted for low-p_T thresholds through the use of all three trigger stations. Studies have shown that this is best achieved using the high-p_T planes TGC1 and RPC3 with appropriate window sizes for the low and high-p_T thresholds.
- In the end-cap an additional coincidence can be required in the planes of the inner TGC chambers, the EI and FI stations, see Figure 11-2.
- In the barrel, trigger electronics and logic are being designed such that signals from the Tile Calorimeter can be input to the trigger and used in coincidence with track candidates from the barrel muon trigger chambers. The Tile Calorimeter offers good separation of muons from hadrons, particularly in its outer depth sampling. Studies have demonstrated that a coincidence makes the trigger robust against the most pessimistic estimates of potential background [11-5]. The resulting rates are discussed in Section 11.3.1.6.

11.3.1.3 Trigger efficiency

The lower momentum limit for detecting a muon in the Muon System is set by the energy loss in the calorimeter and corresponds to p_T ~ 3 GeV in the barrel, but can be as low as p_T ~ 1 GeV in the end-cap. In order to evaluate the level of rejection of muons by the trigger system below a given trigger threshold, single muons over a wide range of momenta were generated in a Monte Carlo program and passed through the detector and trigger simulation programs. The trigger efficiency was evaluated as a function of p_T both for single muons and for muons in physics events, for the combined barrel and end-cap LVL1 trigger system. Since in some regions of the detector (notably in the end-cap) window size and trigger efficiency have some η dependence, the efficiency was evaluated as a function of η (integrated over ϕ). These calculations were performed for pseudorapidities covering the geometrical acceptance of the trigger system. The total trigger efficiency in the region $|\eta| < 2.4$, including geometrical losses, is 79% for 6 GeV muons in the low-p_T trigger with 6 GeV threshold, and 81% for 20 GeV muons in the high-p_T trigger with 20 GeV threshold.

The trigger efficiency was evaluated by simulating the trigger logic using the coincidence windows defined in Section 11.3.1.1. The efficiency, including geometrical acceptance effects, is given by the ratio of the number of triggered muons to the number of generated muons within the η fiducial region. The trigger efficiencies for the combined barrel and end-cap LVL1 system are shown in Figure 11-3 for the 6 GeV low-p_T, and the 20 GeV high-p_T thresholds.

11.3.1.4 Prompt muons and muons from π/K meson decays in flight

The rates for the LVL1 muon trigger were calculated by convolving the cross-section for muon production with the efficiency for a muon to trigger at LVL1. Muons from b and c hadrons, W and Z decays and from decays in flight of charged π and K mesons were considered. In the end-cap the convolution used four η bins to account for the significant η dependence of the cross-section.

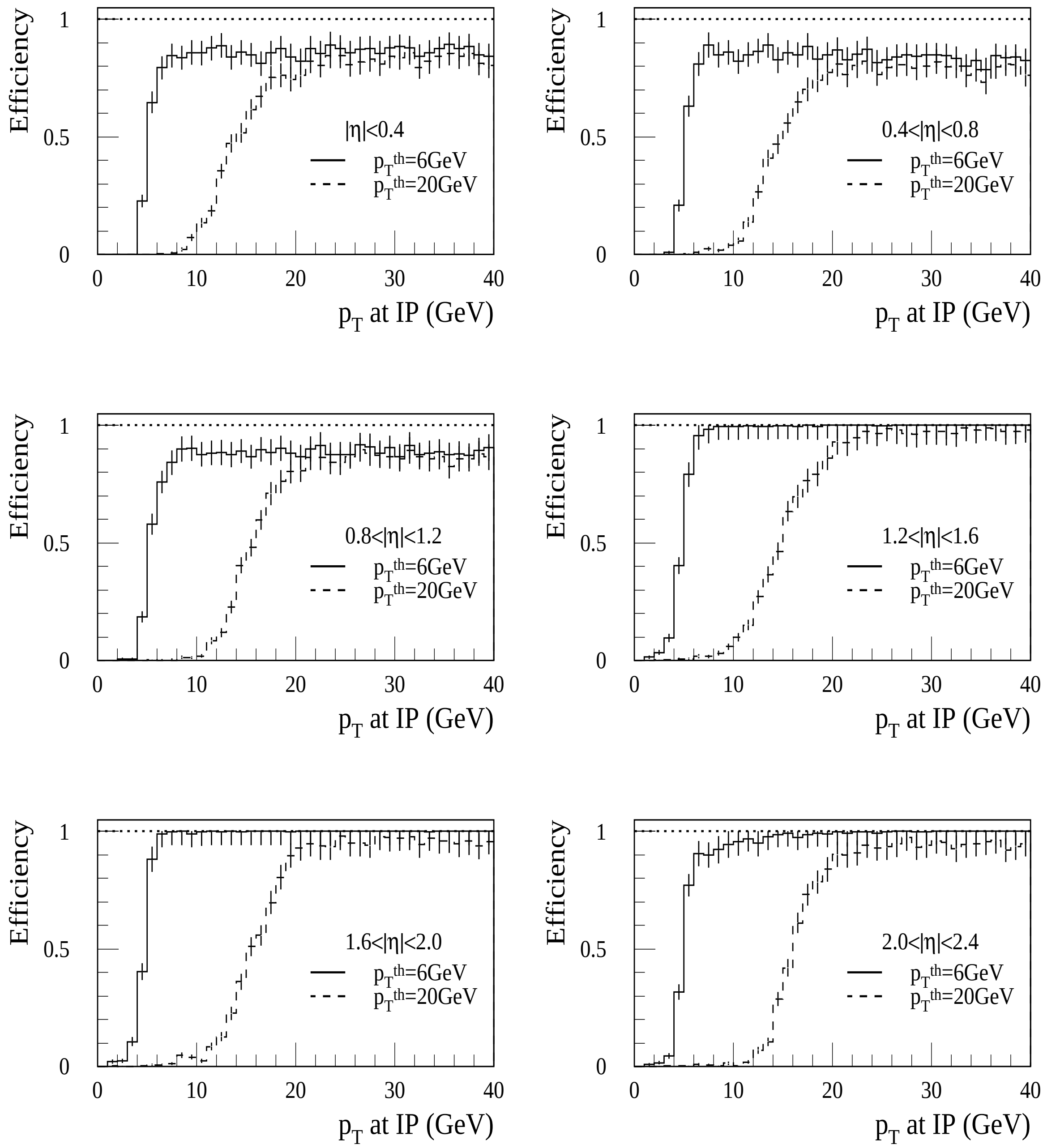

Figure 11-3 The efficiency of the LVL1 muon trigger as a function of p_T and for six pseudorapidity intervals, for the nominal low and high-p_T thresholds of 6 GeV and 20 GeV and the 'TDR trigger scheme' of Section 11.3.1.1. The p_T is given at the interaction point (IP).

The inclusive muon p_T spectrum is dominated, for transverse momenta below 8 GeV, by $\pi/K \rightarrow \mu\nu$ decays. Because of the steeply falling $d\sigma/dp_T$ spectrum, muons with p_T well below threshold still contribute significantly to the trigger rate, despite their low trigger acceptance. At higher p_T, muons from decays of *B*-hadrons are more abundant, and above 30 GeV $W \rightarrow \mu\nu$ decays dominate [11-6]. These rates were calculated using the PYTHIA Monte Carlo program [11-

7]. Because of the significant contribution of π/K decays to the trigger rate, these were calculated using the Monte Carlo program DPMJET [11-8] and using PYTHIA. The predicted rates were found to agree within 30%. The estimated rates are shown in Table 11-3.

Table 11-3 Trigger rates (kHz) expected in the barrel, end-cap and combined Muon System arising from various physics processes. These rates are calculated by convolving the single muon cross-section from each proton–proton process with the efficiency of the LVL1 trigger for single muons. The low-p_T rates assume a luminosity of 10^{33} cm^{-2}s^{-1} and the high-p_T rates a luminosity of 10^{34} cm^{-2}s^{-1}. The Monte Carlo program DPMJET was used for the rates from π/K decays.

Threshold	Process	Barrel	End-cap	Combined system
Low-p_T (6 GeV)	π / K decays	7.0	9.8	16.8
	b	1.9	2.1	4.0
	c	1.1	1.3	2.4
	W	0.004	0.005	0.009
	Total	**10.0**	**13.2**	**23.2**
High-p_T (20 GeV)	π / K decays	0.3	1.8	2.1
	b	0.4	0.7	1.1
	c	0.2	0.3	0.5
	W	0.035	0.041	0.076
	Total	**1.0**	**2.9**	**3.9**

11.3.1.5 Muons from cosmic rays and beam halo

Despite the significant depth at which the ATLAS experiment is located, cosmic rays contribute to the trigger rate in the Muon System. The ATLAS cavern is located about 75 m underground and access is available through two parallel shafts about 60 m deep, and 9 m and 12.6 m in diameter. The cosmic ray rate arises largely from these access shafts. By normalising the incident cosmic rate to 100 Hz / m^2 (the approximate rate of the muon component at sea level), a trigger rate in the low-p_T system below 150 Hz was found. The corresponding rate for the high-p_T system is much lower (< 10 Hz). These rates are two orders of magnitude less than those from muon triggers from *pp* collisions, but still sufficient to be useful for the calibration and alignment of the detectors in the barrel region.

A study of muons produced in interactions between the LHC beam and the machine components has been performed for the CMS experiment using a detailed simulation of such processes [11-9]. The differences between the beam conditions in ATLAS and CMS are sufficiently minor that this simulation is also relevant for ATLAS. The interactions modelled are those of a beam of 530 mA at 7 TeV at high luminosity, with all machine components within 1000 m of the interaction point simulated. The particles produced in these beam-machine interactions are passed through the detector and trigger simulation to estimate the resulting trigger rate in the LVL1 end-cap muon trigger [11-10]. The rates from the estimated muon flux are negligible in comparison with the rate from interaction products, and can contribute significantly to the trigger rate only if the halo rate is underestimated by a factor ten; in this instance the rate is still tolerable. The halo rates are, however, sufficient to be useful for the calibration of the end-cap trigger and for timing studies.

11.3.1.6 Fake muon trigger from hadronic debris

A large background flux is expected in the experimental cavern at the LHC due to the interaction of hadrons (produced in *pp* collisions) with the forward elements of the ATLAS detector, the shielding system and machine elements. The particles produced in such secondary interactions and their decay products can induce high counting rates in the muon trigger system. Here the resulting trigger rate is estimated for the trigger scheme presented in Section 11.3.1.1 and [11-2] ('TDR scheme'). The rate reduction achieved for the more robust scheme (Section 11.3.1.2) is discussed in the next section. The background flux seen in the trigger chambers was evaluated using the FLUKA Monte Carlo program [11-11], which provides a better treatment of low-energy particles down to thermal energies, than the standard ATLAS detector simulation.

Particles of low energy (up to 10 MeV) include mainly soft Compton electrons and neutron-induced soft protons. Such particles produce hits in a single trigger counter (*i.e.* no correlation between trigger planes). This incoherent background was shown to produce triggers at rates much below those expected from *pp* collision products [11-2]. The dominant contribution to the fake low-p_T trigger rate in both barrel and end-cap arises from the coincidence of a pair of hits from a penetrating particle in one of the low-p_T stations, with one or more hits deposited by any other particle. The fake high-p_T trigger rate is dominated by a low-p_T trigger in coincidence with any other hits (or track) in the high-p_T station of the barrel or end-cap.

Harder particles (of momenta above 10 MeV) can give rise to hits in more than one plane of trigger detectors, and thus fake a muon trigger. The majority of such triggers are due to muons of momentum around 100 MeV, arising directly or indirectly from the decay of neutral kaons (*e.g.* $K_L^0 \rightarrow \mu\pi\nu$). This background is therefore called the '100 MeV background'. The K_L^0 flux is produced by interactions of secondaries with the material of the detector, and the forward shielding. The probability for the K_L^0 decay particles with momenta ~100 MeV to give a trigger in the LVL1 system, was calculated by simulating the response of the detector and trigger. The particles generated by FLUKA, which impact on the planes of the trigger detectors, were passed through the standard detector and trigger simulation programs. The resulting fake trigger rates are listed in Table 11-4.

Performance of the improved LVL1 muon trigger

The additional options in the muon trigger discussed in Section 11.3.1.2 have been simulated to demonstrate the gain in trigger robustness against charged particles of momentum ~100 MeV in the ATLAS cavern, as modelled by the FLUKA Monte Carlo program.

The use of the full (three station) logic of the trigger for the low-p_T 6 GeV threshold trigger reduces the expected rate in the end-cap by a factor 4, and in the barrel by a factor ~10. This change requires only minor modification of the trigger electronics and adds considerable robustness.

The additional requirement in the end-cap trigger of a coincidence in the TGC chambers of the EI and FI stations prevents any triggers from muons with momentum too low to penetrate the end-cap toroid, and thus removes triggers from ~100 MeV muons. The occupancy in these chambers then determines the expected trigger rate from accidental coincidences. Depending on the exact form of coincidence, preliminary studies suggest that the probability to validate a fake trigger is approximately 0.7% for low luminosity running (6 GeV threshold) and 0.25% at high luminosity (20 GeV threshold). Such probabilities translate to low trigger rates (see Table 11-4).

Table 11-4 Rates expected in the LVL1 muon trigger from 100 MeV muon flux in the cavern, for various trigger schemes. Safety factors are not taken into account.

	Rate (kHz)	
	low-p_T (6 GeV)	**high-p_T (20 GeV)**
end–cap		
TDR scheme	7.8	6.4
three station logic	1.8	6.4
coincidence with EI/FI	0.05	0.02
barrel		
TDR scheme	6.8	<1.0
three station logic	0.5 – 1.0	<1.0
coincidence with Tile Calorimeter	<0.27	<0.04

In the barrel, a preliminary study of the stand-alone muon identification capability of the Tile Calorimeter indicates that the probability for a hadron to fake a muon signal in the calorimeter is low [11-12]. In an additional study a single muon of 20 GeV was added to pile-up events corresponding to high luminosity. The E_T deposited in a cone ($\Delta\eta\times\Delta\phi$ = 0.4×0.3) around the muon and the E_T in a cone not containing the muon was compared for two cases: summation of all samplings in depth or using only the outer sampling. For a muon efficiency of 99% the probability to fake a muon signal was found to be ~1% in both cases (see Section 5.3.3).

The efficiency of the more robust trigger for both low and high-p_T thresholds is comparable to that of [11-2] – the criterion of 90% acceptance of muons at these thresholds is largely maintained. Use of the EI and FI chambers of the TGC in the LVL1 trigger will reduce efficiency below 90% in some regions due to the incomplete ϕ coverage of the forward chambers. The expected rates arising from fake muons in the improved trigger schemes are listed in Table 11-4. These values are tolerable in terms of the maximum rate which the LVL1 and LVL2 triggers can accept, even allowing for safety factors of ~10. Uncertainties in these rates arise largely from assumptions made in the Monte Carlo simulation used to model the backgrounds, and are estimated to be smaller than this safety factor. Additional substantial uncertainties are due to statistical uncertainties arising from the weighting procedure for the Fluka Monte Carlo sample.

In conclusion, if backgrounds are as predicted by the Monte Carlo, it will be sufficient to use only the three-station logic, low-p_T trigger scheme in both barrel and end-cap. The option of including the EI/FI coincidence in the end-cap and the Tile coincidence in the barrel provides a very robust trigger.

11.3.2 LVL1 calorimeter triggers

The input to the calorimeter LVL1 algorithms are a set of 'trigger towers' of granularity 0.1×0.1 in $\Delta\eta\times\Delta\phi$. These are formed by analog summation of calorimeter cells. There are separate sets of trigger towers for EM and hadronic Calorimeters [11-2]. Truncating the digitised values for the tower energies to eight bits effectively applies a 1 GeV threshold to each trigger tower.

11.3.2.1 Electron/photon trigger

The LVL1 electron / photon trigger algorithm is based on a window of 4×4 towers in the electromagnetic and hadronic calorimeters in the region $|\eta| < 2.5$, and consists of four elements:

- a 2×2-tower EM cluster, used to identify the position of candidate RoIs (local E_T maximum);
- a 2×1 or 1×2-tower EM cluster, used to measure the E_T of EM showers – there are four such regions within the RoI cluster, and the most energetic of these is used;
- a ring of 12 electromagnetic towers surrounding the clusters, which is used for isolation tests in the EM Calorimeter;
- the 16 hadronic towers behind the electromagnetic clusters and isolation ring, which are used for isolation tests in the hadronic calorimeters.

The window slides in steps of one trigger tower in both the η and ϕ directions.

It is foreseen that electron / photon candidates may contribute to the LVL1 trigger in three ways: as inclusive triggers, where at least one signal above a given threshold is sufficient to cause an event to be accepted; in electron / photon multiplicity triggers, *e.g.* dielectron / diphoton triggers; and in combination with other trigger inputs, *e.g.* electron and missing-E_T or electron and muon.

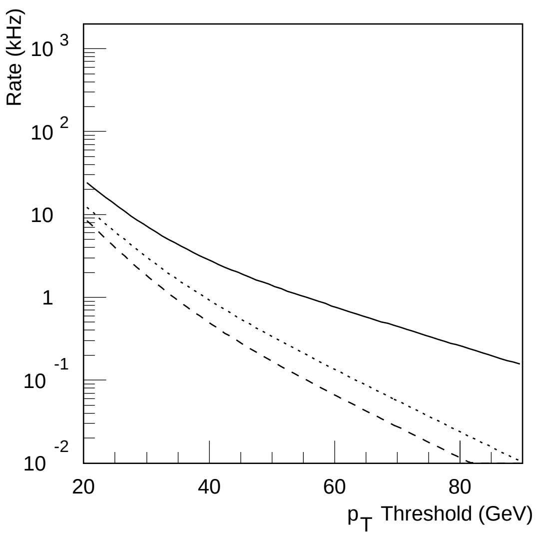

Figure 11-4 Inclusive electron trigger rate for luminosity 10^{33} cm^{-2}s^{-1}, without isolation (solid), requiring only hadronic isolation (dotted) and requiring both electromagnetic and hadronic isolation (dashed).

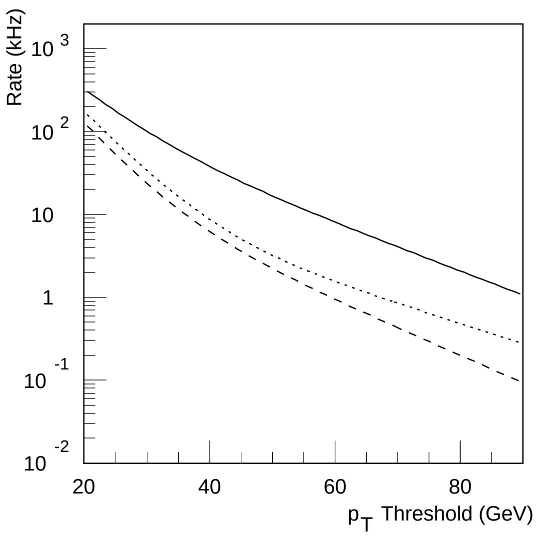

Figure 11-5 Inclusive electron trigger rate for luminosity 10^{34} cm^{-2}s^{-1}, without isolation (solid), requiring only hadronic isolation (dotted) and requiring both electromagnetic and hadronic isolation (dashed).

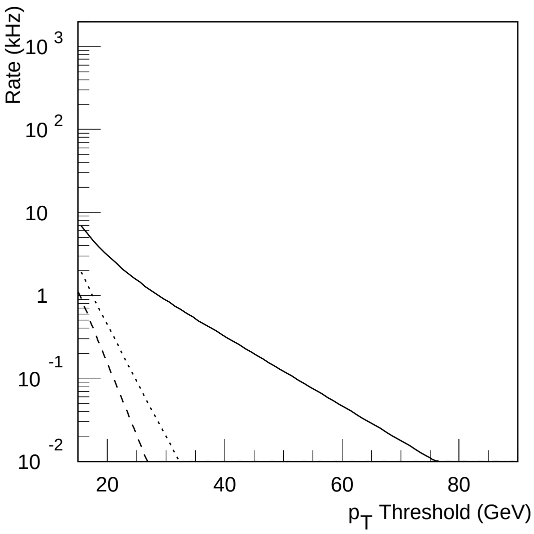

Figure 11-6 Electron/photon pair trigger rate for luminosity 10^{33} cm^{-2}s^{-1}, without isolation (solid), requiring only hadronic isolation (dotted) and requiring both electromagnetic and hadronic isolation (dashed).

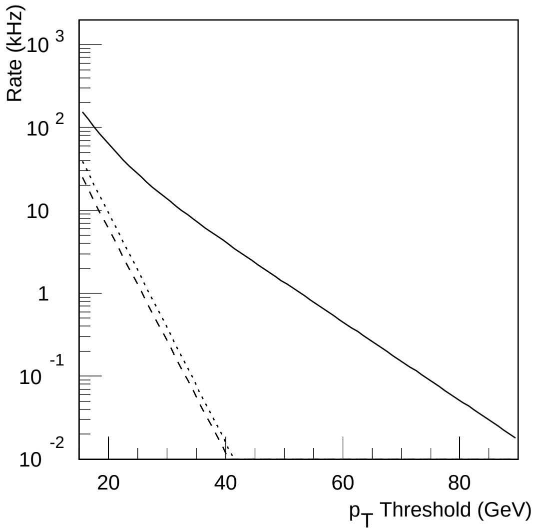

Figure 11-7 Electron/photon pair trigger rate for luminosity 10^{34} cm^{-2}s^{-1}, without isolation (solid), requiring only hadronic isolation (dotted) and requiring both electromagnetic and hadronic isolation (dashed).

Figures 11-4 and 11-5 show the estimated inclusive trigger rates as a function of the actual trigger threshold for 95% electron efficiency at the threshold value, for luminosities of 10^{33} cm^{-2}s^{-1} and 10^{34} cm^{-2}s^{-1}. Each plot shows the rate without isolation, using only hadronic isolation, and using both electromagnetic and hadronic isolation. Figures 11-6 and 11-7 show similar distributions for a dielectron / diphoton trigger. In these, the isolation cuts were chosen to give 95% efficiency for triggering on the pair, rather than a single electron or photon.

There is a dependence of isolation E_T on electron / photon E_T, and so one would not require the same isolation thresholds for different values of cluster E_T. Also, since the trigger rate falls quite rapidly with increasing cluster E_T, there is no need to require stringent isolation for higher-E_T clusters, as the effect on trigger rate is negligible. It is therefore anticipated that the isolation requirements will be progressively loosened with increasing cluster E_T. An example of this is shown in Table 11-5 for low luminosity, and in Table 11-6 for high luminosity.

Table 11-5 An example of how isolation criteria might be progressively loosened with increasing E_T for luminosity 10^{33} cm^{-2}s^{-1}. The total rate is less than the sum of the parts due to overlaps between the different selections. The thresholds listed are those actually applied and are lower than the 'nominal trigger threshold' to guarantee 95% efficiency above the 'nominal threshold'.

Trigger selection	Threshold	Isolation	Rate
≥ 1 electron / photon	E_T > 17 GeV	EM + hadronic	11 kHz
≥ 1 electron / photon	E_T > 35 GeV	hadronic	1.2 kHz
≥ 1 electron / photon	E_T > 60 GeV	none	0.6 kHz
≥ 2 electron / photons	E_T > 12 GeV	EM + hadronic	1.4 kHz
≥ 2 electron / photons	E_T > 20 GeV	hadronic	0.1 kHz
≥ 2 electron / photons	E_T > 35 GeV	none	0.3 kHz
Total trigger rate			**13 kHz**

Table 11-6 An example of how isolation criteria might be progressively loosened with increasing E_T for a luminosity 10^{34} cm^{-2}s^{-1}. The total rate is less than the sum of the parts due to overlaps between the different selections.

Trigger selection	Threshold	Isolation	Rate
≥ 1 electron / photon	E_T > 26 GeV	EM + hadronic	21.5 kHz
≥ 1 electron / photon	E_T > 45 GeV	hadronic	2.6 kHz
≥ 1 electron / photon	E_T > 75 GeV	none	3.0 kHz
≥ 2 electron / photons	E_T > 15 GeV	EM + hadronic	5.2 kHz
≥ 2 electron / photons	E_T > 25 GeV	hadronic	0.4 kHz
≥ 2 electron / photons	E_T > 45 GeV	none	1.5 kHz
Total trigger rate			**29.2 kHz**

11.3.2.2 τ / hadron trigger

The LVL1 τ / hadron trigger can be implemented at relatively little additional cost, using the same input and much of the same logic used for the electron / photon trigger. The algorithm starts from a 4×4 trigger-tower block and requires that the central 2×2 trigger-tower block, summing over EM and hadronic layers, contains more E_T than any of the other eight possible 2×2 tower blocks in the same 4×4 window. This 2×2 block slides by 0.1 in both η and ϕ direction. The core energy is defined as the maximum energy in a 2×1 EM region (within the 2×2 area) plus the 2×2 hadronic block.

For the isolation definition, the 12 trigger towers surrounding the 2×2 core are used, summing the towers in the EM and hadronic Calorimeters separately. The isolation in τ events was compared to that in jet events separately for the EM and hadronic layers. The EM isolation is much more powerful than the hadronic one. The isolation sum in the hadronic layer may also be used, but its discrimination power is not very large.

In order to evaluate the efficiency as a function of E_T, the summed E_T of the hadronic daughters of the τ was used rather than the E_T of the τ itself. The efficiency for the τ events versus this τ hadronic E_T is depicted in Figure 11-8 for a low and a high threshold.

Figure 11-9 shows the absolute trigger rate that would result from using the τ / hadron trigger in a stand-alone way as a function of core-E_T threshold, assuming a luminosity of 10^{33} cm^{-2}s^{-1}. The effect of pile-up has been neglected. The figure shows the rate with and without an electromagnetic isolation cut, where two possibilities are indicated for the dependence of such an isolation cut on the core threshold. The first possibility is no dependence – *i.e.* a fixed cut, while the second possibility is a direct proportionality with the core threshold. The optimal choice probably lies somewhere in between these extremes.

11.3.2.3 Jet trigger

Jet production is expected to be the dominant hard process at the LHC. Unlike the electron / photon and τ / hadron triggers, the main requirement on the jet trigger is therefore not that it should discriminate between two different types of objects, but rather that it should discrimi-

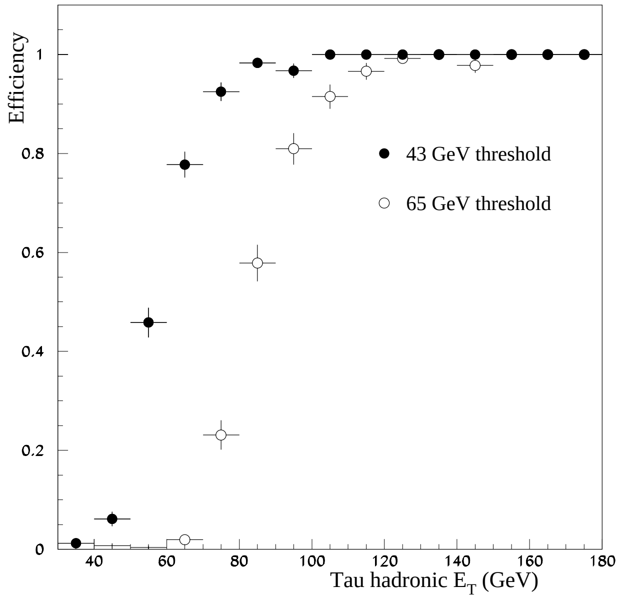

Figure 11-8 Efficiency versus τ hadronic E_T (in GeV) for a low and a high threshold as indicated. No isolation was required.

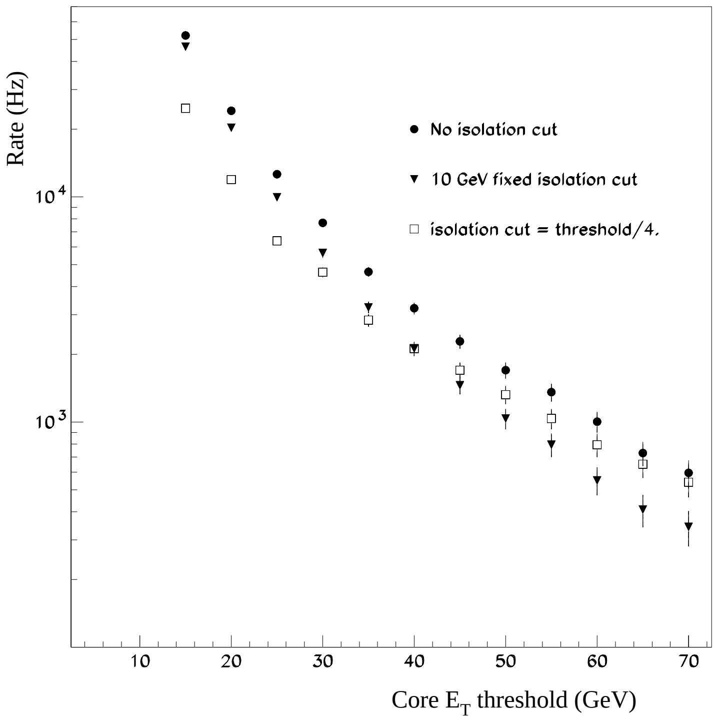

Figure 11-9 Trigger rate vs core-E_T threshold for an inclusive τ trigger, assuming a luminosity of 10^{33} $cm^{-2}s^{-1}$ neglecting pile-up. The effect of using an electromagnetic isolation requirement is indicated.

nate on the basis of the E_T and multiplicity of jets. Only when trying to flag the lowest–E_T jets (20–40 GeV) as secondary RoIs for LVL2, is the question of background from other sources (noise and pile-up) expected to be relevant.

For most of the studies a 'fast' simulation was used. This included a realistic model of the electronics effects, preprocessing and trigger algorithms, but lacked the detailed simulation of the detector and material. This model allowed large, high-E_T datasets to be produced easily. Cross-checks were performed using the full GEANT-based simulation, particularly in the area of low-E_T jet performance, see Section 9.1.

A problem with jet trigger studies is that there is no unique definition of what constitutes a 'jet'. Hence one must use a particular jet-finder as a 'reference' against which the trigger algorithms are compared. Fixed-cone algorithms are widely used, but relying on one of these as a reference carries the risk that it would bias studies of the optimum cluster size. For this reason, both a fixed cone algorithm (with R = 0.4) and a k_T algorithm [11-13] were used as references for comparison with the trigger algorithms. The plots shown are for the k_T algorithm, but the results did not significantly depend on which algorithm was used.

The jet trigger algorithm is based on a window of 'jet elements', which have a granularity of 0.2×0.2 in $\Delta\eta\times\Delta\phi$ and are summed in depth between the EM and hadronic Calorimeters. The algorithm has two components, consisting of a 2×2-element cluster, used to identify the position of candidate jet RoIs (local E_T maximum), and a trigger cluster, used to measure the jet E_T. This cluster can be 2×2, 3×3 or 4×4 jet elements (0.4×0.4, 0.6×0.6 or 0.8×0.8 in $\Delta\eta\times\Delta\phi$), where the choice is programmable separately for each threshold setting. The window slides in steps of 0.2 (one element) in both the η and ϕ directions for $|\eta| < 3.2$.

The optimum size of the jet cluster depends on both the jet E_T and the luminosity. The resolution for high-E_T jets at low luminosity is dominated by the containment of the jet E_T within the cluster, favouring a larger cluster. Conversely, when flagging low-E_T jets, especially at high luminosity, the amount of electronic and pile-up noise within the jet cone is the limiting factor in jet trigger performance. For this reason, a flexible system is foreseen, in which different jet cluster sizes may be used simultaneously at different E_T thresholds, allowing optimisation of different jet selections for different purposes. Table 11-7 summarises the jet cluster sizes which are recommended for different jet trigger types; for a detailed discussion see [11-1], Section 6.4.

Table 11-7 Recommended window sizes for different jet trigger types.

Trigger type	Jet cluster size
high-E_T single jet trigger	0.8×0.8
low-E_T single jet trigger	0.4×0.4
multi-jet trigger (≥ 3 jets)	0.4×0.4

Figure 11-10 shows the threshold efficiency curves for 100 GeV E_T jets for different cluster sizes, at a luminosity of 10^{33} cm^{-2}s^{-1}. Such jets are of interest for the inclusive jet trigger at this luminosity. As can be seen, the threshold sharpness for jets of 0.6×0.6 and 0.8×0.8 is very similar, while the smaller 0.4×0.4 cluster produces a much softer threshold. Figure 11-11 shows the dependence between efficiency for these jets and the inclusive trigger rate for the same algorithms. From this it can be seen that the larger clusters produce a lower rate when high efficiency is required. The same quantities are shown in Figures 11-12 and 11-13 for 200 GeV E_T jets at the high luminosity of 10^{34} cm^{-2}s^{-1}. Again, a larger cluster size is favoured.

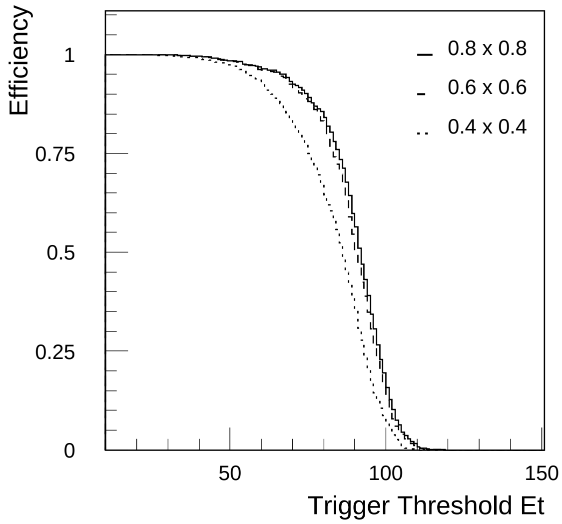

Figure 11-10 Jet trigger efficiency curves for 100 GeV E_T jets, for different cluster sizes, at luminosity 10^{33} cm^{-2}s^{-1}. The efficiency is shown as function of the actual trigger threshold (in GeV).

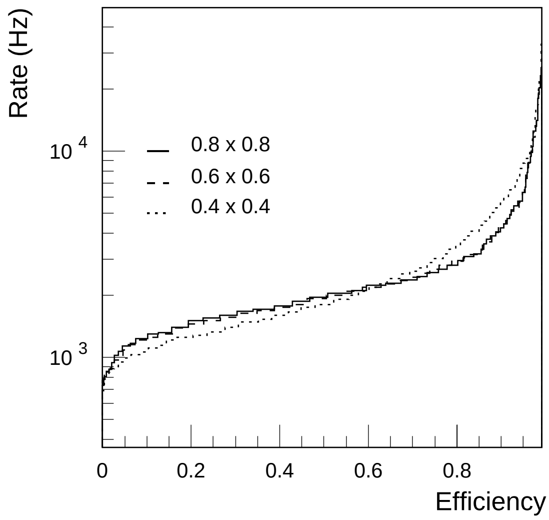

Figure 11-11 Trigger rate versus efficiency for 100 GeV E_T jets, for different cluster sizes, at luminosity 10^{33} cm^{-2}s^{-1}.

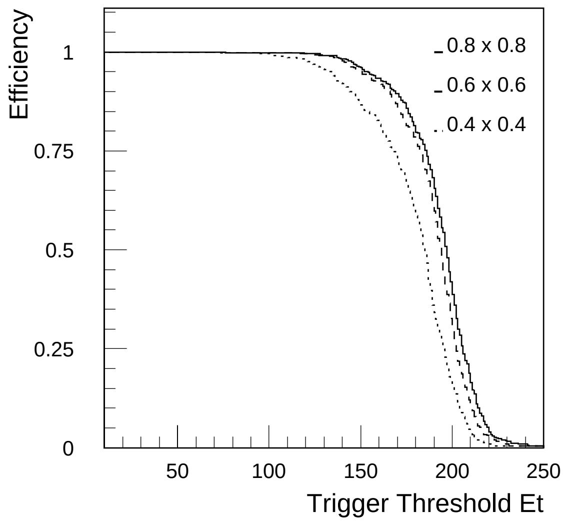

Figure 11-12 Jet trigger efficiency curves for 200 GeV E_T jets, for different cluster sizes, at luminosity 10^{34} cm^{-2}s^{-1}.

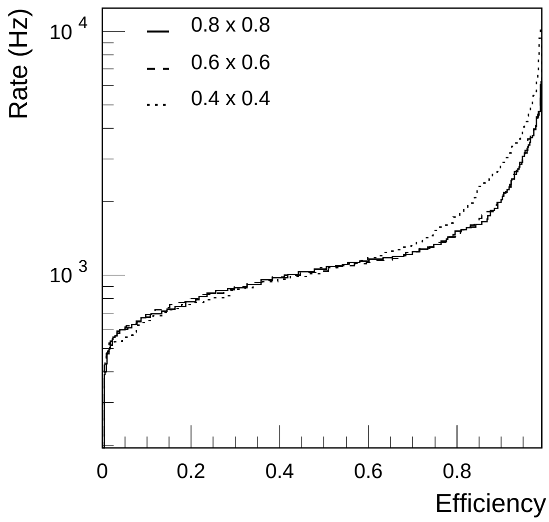

Figure 11-13 Trigger rate vs. efficiency for 200 GeV E_T jets, for different cluster sizes, at luminosity 10^{34} cm^{-2}s^{-1}.

While the resolution for inclusive high-E_T jets depends primarily on the trigger cluster size, the RoI coordinate resolution and the ability to resolve nearby jets depend on the step size and RoI definition. Better resolution is obtained from a smaller RoI cluster. The smaller RoI cluster also results in a higher efficiency to resolve nearby jets. This affects the acceptance of a multi-jet trigger, and the ability to count jets in events with complex topologies.

In addition to providing signals for use in inclusive jet triggers, multi-jet triggers, and combined triggers (such as jet and missing-E_T), the jet trigger system should flag ‘secondary jet RoIs’ which might be useful for more refined event selections at LVL2. Such jets are of lower E_T. It is important to understand the ability of LVL1 to flag very low-E_T jets. Figure 11-14, shows the efficiency for the trigger to find an RoI matched to a reference jet as a function of jet E_T, for a trigger threshold chosen to give an average RoI multiplicity in electron / photon-triggered events (assumed to dominate in the LVL1 trigger rate over jet triggers) of about three RoIs / event for a luminosity of $10^{33}\ \mathrm{cm}^{-2}\mathrm{s}^{-1}$. It suggests that efficient identification of 20 GeV jet RoIs might be possible at low luminosity, but lower-E_T jets would be difficult. Figure 11-15 shows similar distributions at $10^{34}\ \mathrm{cm}^{-2}\mathrm{s}^{-1}$. Here, the use of a smaller cluster (0.4×0.4) is compared to the application of a threshold to the jet-element E_T, both done in order to suppress the contribution from pile-up. It can be seen that these techniques can improve the RoI efficiency at low jet E_T.

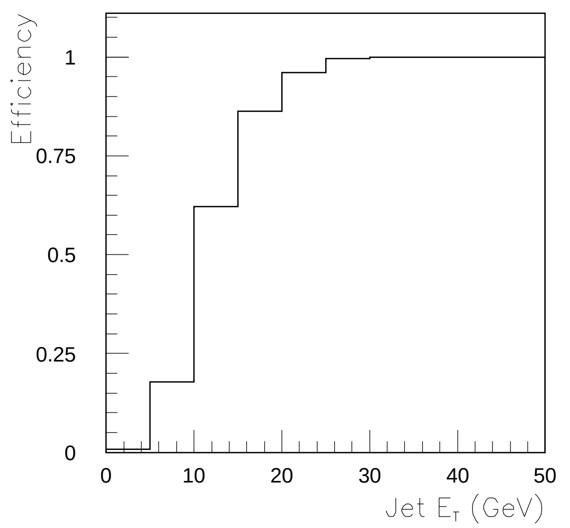

Figure 11-14 Efficiency to flag a jet RoI as a function of jet E_T.The trigger threshold was chosen to give an average RoI multiplicity in electron/photon-triggered events of about three per event. The algorithm used was a cluster of 0.8×0.8, sliding by 0.2 (luminosity $10^{33}\ \mathrm{cm}^{-2}\mathrm{s}^{-1}$).

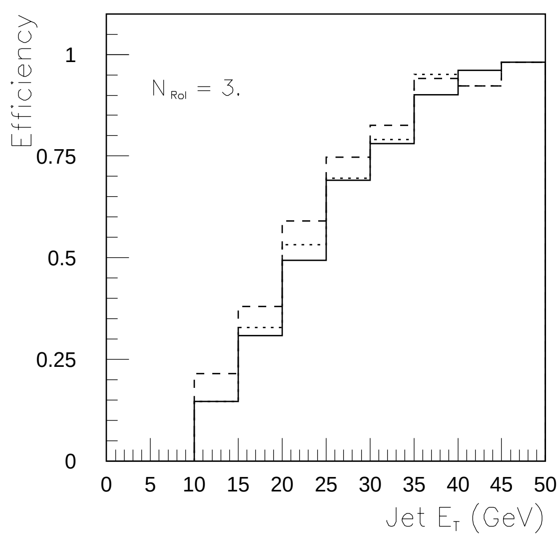

Figure 11-15 Efficiency to flag a jet RoI as a function of jet E_T, at luminosity $10^{34}\ \mathrm{cm}^{-2}\mathrm{s}^{-1}$. The histograms compare a jet of 0.8×0.8 with no threshold on jet-element E_T (solid), the same cluster but using only elements with $E_T \geq 3$ GeV (dashed), and a jet of 0.4×0.4 (dotted).

The following figures demonstrate the overall performance of the jet trigger. Figure 11-16 shows the estimated inclusive jet trigger rates as a function of trigger threshold for the three window sizes, for luminosity of $10^{33}\ \mathrm{cm}^{-2}\mathrm{s}^{-1}$. Similarly, the estimated three-jet trigger rates are shown in Figure 11-17. Trigger rates of around 1 kHz can be obtained for inclusive jet thresholds of 100-110 GeV at low luminosity or 190–200 GeV at high luminosity.

In fact, rates substantially lower than this may be required in the LVL1 jet trigger. This is because LVL2 can provide only a modest rejection against LVL1 jets, and so a few kHz LVL1 jet trigger rate would saturate the output of the LVL2 system unless additional criteria are applied at LVL2 to reject events. Allocating 200 Hz rate for each of the inclusive, three-jet and four-jet triggers, the resulting trigger thresholds at low and high luminosity are shown in Table 11-8.

11.3.3 Missing transverse energy and total transverse energy triggers

For the missing transverse energy and total transverse energy triggers the calorimeter energies are summed into a map with a granularity of $\Delta\eta\times\Delta\phi = 0.2\times0.2$, which is the same as for the jet processor for $|\eta| < 3.2$; the map for missing-E_T extends over the largest possible η range,

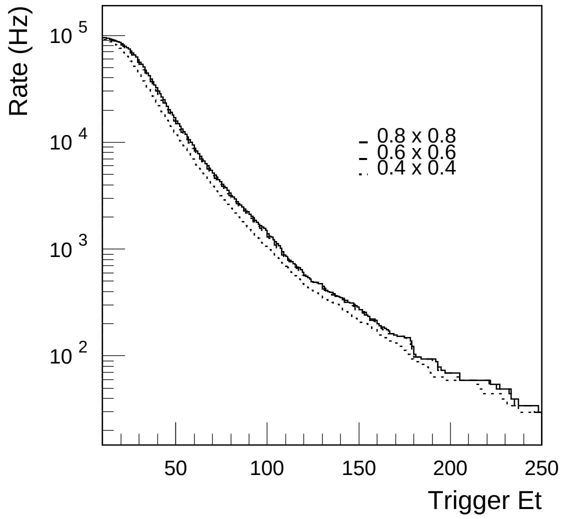

Figure 11-16 Inclusive jet trigger rates versus trigger E_T threshold (in GeV) at $L = 10^{33}\ cm^{-2}s^{-1}$. Curves are shown for the three different cluster sizes available to the trigger and as functions of the actual trigger threshold.

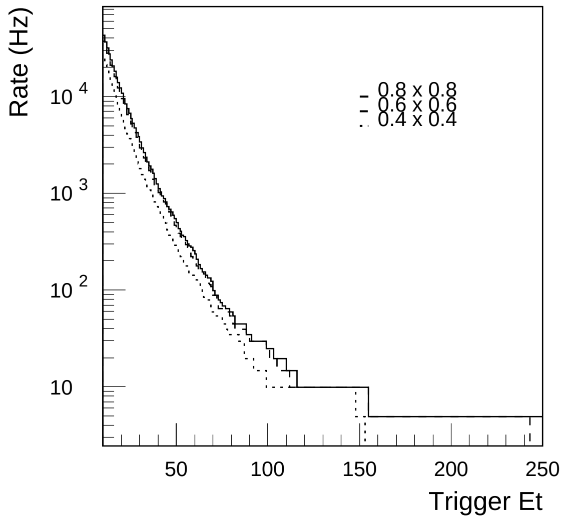

Figure 11-17 Three-jet trigger rates versus trigger E_T threshold at $L = 10^{33}\ cm^{-2}s^{-1}$. The rates are shown as functions of the actual trigger threshold. The bins above 150 GeV contain very low statistics.

Table 11-8 Jet E_T thresholds for 200 Hz LVL1 trigger rate, for single, three and four-jet triggers, at low and high luminosity. The E_T threshold is the E_T of the jet for which the trigger is 95% efficient, with a 'jet' being defined as described in the text.

Trigger type	**Low luminosity ($10^{33}\ cm^{-2}s^{-1}$)**	**High luminosity ($10^{34}\ cm^{-2}s^{-1}$)**
Single-jet	E_T > 180 GeV	E_T > 290 GeV
Three-jets	E_T > 75 GeV	E_T > 130 GeV
Four-jets	E_T > 55 GeV	E_T > 90 GeV

$|\eta| < 4.9$. The total scalar E_T, as well as the components E_x and E_y in the plane transverse to the beam axis, are computed. Although the missing-E_T trigger itself is not included in the basic LVL1 inclusive triggers, its combination with the single-jet, electron/photon, and τ/hadron triggers is important to allow triggering on interesting events with low jet, e/γ or τ/h transverse-energy thresholds.

The missing-E_T resolution is dominated by the calorimeter resolution and response, and by the addition of electronic noise in the tower-builder electronics. The dependence of the resolution, represented by the rms of E_x, on the value of total scalar E_T, is shown in Figure 11-18. Truncating the digitised values for the tower energies to eight bits effectively applies a 1 GeV threshold to each trigger tower, which reduces the noise contribution to the resolution, which is important for low values of scalar E_T. The degradation observed at very high total E_T is due to the limit in dynamical range (256 GeV per trigger element) and has no impact on the physics since such events are selected anyway by other triggers.

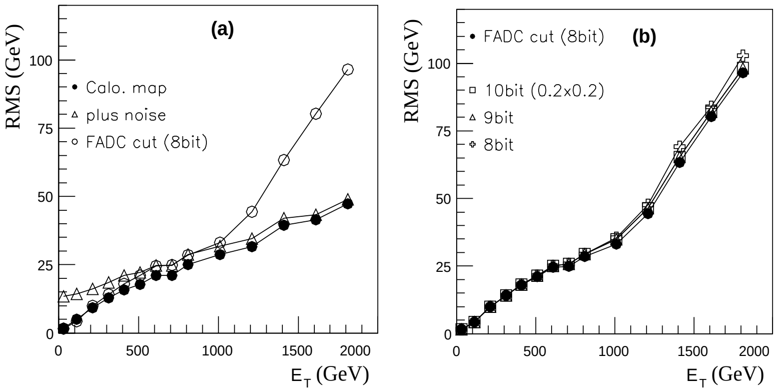

Figure 11-18 Dependence of the resolution of the E_x, E_y components of the total transverse momentum on total E_T. (a) after the trigger preprocessor, in comparison to the resolution obtained at the calorimeter level, using the trigger tower granularity for the E_T calculation; (b) after the transmission of the summed 0.2×0.2 element energies to the Jet/Energy-sum Processor, using 8, 9 (default), or 10 bits.

The inclusive missing-E_T trigger rate is dominated by QCD di-jet events and pile-up. At low luminosity the presence of pile-up (average 2.3 events) increases the trigger rate by about a factor five for $E_T^{miss} < 60$ GeV. Above about 100 GeV, low-luminosity pile-up has no influence. At high luminosity, however, the rate increases by a factor of ~10^3 at E_T^{miss} ~ 100 GeV, and by about a factor 10 at 200 GeV [11-14].

For processes with a genuine missing-E_T signature the combination of the E_T^{miss} trigger with the EM cluster and / or jet triggers allows reduction of the EM and / or jet thresholds. High signal efficiency can be retained at low luminosity for $W \rightarrow e\nu$ and $t\bar{t}$ events. For high luminosity the thresholds have to be raised, and rates are manageable only for signal efficiencies of about 50% for W and $t\bar{t}$. A trigger with a moderate E_T^{miss} threshold together with two jets, results in an efficient SUSY trigger, both at low and high luminosity. Details of combined triggers are discussed in [11-14]. Figure 11-19 demonstrates the usefulness of the E_T^{miss} signature for a trigger aimed at SUSY channels (SUGRA point 2 and 3, see Chapter 20) for low and high luminosity, respectively.

11.4 LVL2 RoI-guided triggers

11.4.1 Overview of algorithms

Higher-level triggers must reduce the LVL1 rate of up to 100 kHz to about 100 Hz, where the largest rejection is expected from the LVL2 trigger. The processing steps at LVL2 are as follows. Raw data associated with the RoIs indicated by LVL1 are collected and prepared. Feature extraction (FEX) is performed for each detector system, starting with the confirmation of the LVL1 RoI in the system from which it originated (Muon System or calorimeter), followed by confirmation in other systems, for example the tracking systems. Features from different systems are combined, to form identified LVL2 trigger objects, which are candidates for muons, electrons, photons, τ's, and jets, as well as generalised missing-E_T and B-physics objects. A global decision is taken based on trigger menus, see Section 11.7.3.

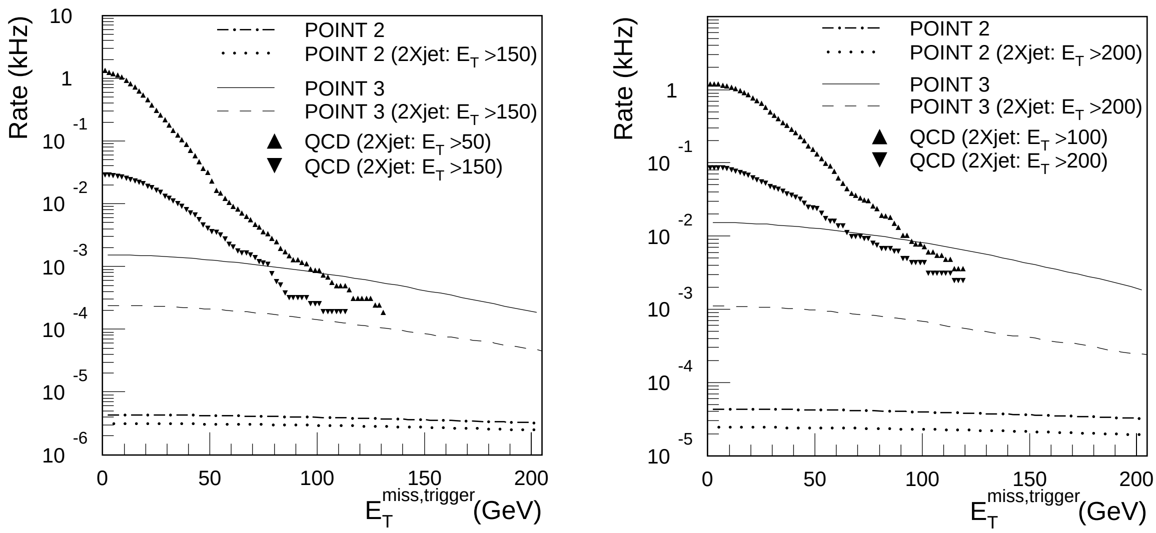

Figure 11-19 LVL1 inclusive E_T^{miss} and combined E_T^{miss}+jet trigger rates for two SUSY points and the QCD background jets. The rates are shown as function of the E_T^{miss} trigger threshold for low (10^{33} cm^{-2}s^{-1}) and high luminosity (10^{34} cm^{-2}s^{-1}) in the left and right figure, respectively.

An average processing time of ~10 ms per event is currently assumed for the LVL2 trigger. The FEX algorithms are at the heart of the LVL2 trigger processing. The performance obtained in efficiency and background-rejection power determines the overall performance of the LVL2 trigger. The data-collection and preprocessing step, which preceeds feature extraction, is important and may be time consuming, but the bulk of the algorithmic complexity lies in the feature extraction. The subsequent object-building step, as well as the global-decision algorithm, is comparatively simple. The special case of *B*-physics triggers is discussed separately in Section 11.6.

The algorithms presented here are prototypes for the ones that will finally be used. They demonstrate the feasibility of obtaining the required trigger performance, while being simple enough to be implemented in the LVL2 trigger. Based on initial timing studies with these algorithms, one can be confident that they are fast enough to be used in the trigger. More work is required, however, to obtain realistic ‘benchmark’ figures on execution time (in the present software environment there are unnecessary overheads, related for example to diagnostic facilities).

The key requirements common to all algorithms are:

- high efficiency for the signal processes, larger than 95% per RoI relative to the LVL1 selection;
- uniform efficiency in η and constant or increasing efficiency with increasing E_T above threshold, which is difficult to achieve in certain regions of the detector, such as the barrel/end-cap overlap regions or where support structures obstruct the acceptance (these regions may be excluded from this requirement);
- reduction of the background rate. This is achieved by improved object identification and sharper thresholds, and implies good p_T resolution and small rates of fake objects;
- robustness with respect to luminosity;

- robustness with respect to noise, dead channels, imperfections of calibration and alignment constants, within the limits expected for the preliminary values available to the trigger.

The key selection criteria are functions of luminosity, E_T (or p_T), and location in the detector (mainly pseudorapidity), and may vary depending on the trigger menu. For example, looser selections may be applied to electron candidates in di-electron triggers than for single electron triggers. In this multi-dimensional parameter space, the operating point is chosen so as to achieve the required efficiency. Other choices could be the optimisation of the number of correctly reconstructed and tagged events relative to the number of background events. Such studies are part of the overall optimisation of the trigger implementation, taking into account processing power, data bandwidth and cost requirements, which is a joint task of the LVL2, EF, physics and trigger-performance groups. The FEX algorithms and the global algorithms were presented previously in detail in Chapters 8 and 9 of [11-1]. In this document, the FEX and global algorithms are described together, and only summaries of the results are reported here.

In the case of the muon trigger, the techniques to reduce the rate from LVL1 are described in Section 11.4.2 and use data from the muon spectrometer to remove fake LVL1 triggers resulting from noise hits due to radiation in the cavern and will reduce the rate by making a sharper p_T cut. Further rate reduction can be expected from using the Inner Detector to sharpen the p_T cut and to remove some of the background from decays in flight of pions and kaons by requiring a good match between the tracks reconstructed in the Inner Detector and the muon spectrometer. These studies are at an early stage and are at present only available for offline reconstruction, see Chapter 8. A larger rejection factor is expected from requiring isolation of the muon using information from the calorimeters as discussed in Section 11.4.2.2.

The photon trigger (Section 11.4.3.2) uses calorimeter features to reduce the background from jets and preserve high efficiency for $H \to \gamma\gamma$ events. For the electron trigger, a large background-rejection factor can be obtained by combining the features from the calorimeter and the Inner Detector as discussed in Section 11.4.3.3. Similarly, background to the τ trigger can be reduced by requiring the presence of a track matched to the calorimeter cluster (Section 11.4.4).

Improvement of the jet trigger is possible for low-E_T jets, but is marginal for high-E_T jets (see Section 11.4.5). In Section 11.4.6, a preliminary study of a possible *b*-jet tag trigger, based on impact-parameter measurements, is presented.

11.4.2 Muon trigger

11.4.2.1 Muon identification in the Muon System

The purpose of the LVL2 muon trigger is the identification of the muon tracks, the accurate calculation of the position and transverse momentum in the muon spectrometer, and the extrapolation to the Inner Detector and calorimeter. The following presents the LVL2 muon algorithm, which was shown to be applicable for low and high thresholds and for both the barrel and end-cap system [11-15]. Note that if a muon candidate does not pass the p_T threshold, it may still be of interest as a soft muon candidate, when the event is selected by other triggers.

The Muon System consists of sets of chambers, which are arranged in superlayers (SL, inner, middle, outer). Each chamber has two groups of multi-layers, built from three to four layers of MDT tubes each. The LVL1 trigger function is provided by three layers of RPCs or TGCs. In the barrel the first two trigger layers are located around the MDT chambers in the middle station and the third layer is located above or below the outer MDT station. In the end-cap a TGC is placed in front of the middle MDT chambers and two TGCs are placed behind them (see Figure 11-2).

The high-background environment in the Muon System requires algorithms with high capability of rejecting background hits due to the activity accompanying the muon track and the soft background in the cavern. Hits from the fast detectors of the LVL1 muon trigger (RPC and TCG), which have very low occupancy, are used to refine the road provided by LVL1. Next, a local track reconstruction is performed to determine a 'superhit' in a given MDT multi-layer. The superhits of the track are assembled to determine the radius of curvature of the candidate track. The momentum is found by matching the reconstructed track with patterns of tracks stored in a fine-grained lookup table. Many tracks, especially in the barrel / end-cap transition region, have complicated chamber hit patterns, which can change rapidly as a function of momentum, η or ϕ. The radius method is a means to use all hit–chamber information in a manner roughly independent of where the super points are actually located.

The first stage of the LVL2 trigger is the refinement of the RoI region. For the barrel the RPC hits bracketing the middle superlayer and the RPC hits in the outer superlayer, if they exist, are used to reconstruct a circular trajectory. This trajectory is used to determine the RoI in the first superlayer and refine the RoI in the middle and outer superlayers. If the outer SL hits do not exist, a rough fit of a circle is performed under the assumption that the muon trajectory in the (R, z) plane is a straight line from the IP up to the first SL. For the end-cap system the refined RoI is determined by a circular fit through the end-cap toroid using TGC hits to fix the tangent line and the IP to determine the position in the first SL. The actual width of the refined RoI is adjusted according to the quality of the fit of the trajectory. For a good quality fit the roads are two to three MDT tubes wide.

The next stage of the LVL2 trigger formation involves the recognition of tracks in a given MDT multi-layer within the refined RoI road. This is accomplished by means of an *ad hoc* quality factor developed from an adjacency test (a type of Hough transformation) and a χ^2 consistency test on all tangent lines of all pairs of hit tubes consistent with broad limits of extrapolation back to the interaction point.

The coordinate along the sense wires (s-coordinate) is determined by the trigger-chamber system. It is assumed that each trigger hit furnishes a space point, *i.e.* that the two planar coordinates are correctly associated at the raw-data level. Each space point is converted to the polar angle ϑ, which is fitted in the end-caps as a function of z (along the beam), or, in the case of the barrel, as a function of x (local coordinate perpendicular to barrel chamber planes). Knowledge of the ϑ-dependence allows the s-coordinate to be estimated by extrapolating to the MDT plane.

Space points are reconstructed from the MDT and trigger planes, although only the MDT information is used to determine the muon trajectory in the bending plane. Given that the trigger planes have a rather coarse segmentation, yielding second-coordinate resolution of 5 to 10 mm, only MDT hits for the same chamber central angle ϕ_0 are used in most cases. All the MDT chamber planes are employed, however, for tracks with fewer than four MDT planes at the same ϕ_0.

The information needed for momentum determination is the curvature of the track and the magnetic-field integral. The momentum at the interaction point is determined by scaling the reconstructed track radius to the radius of the four nearest calibration tracks which are averaged by linear weighting of the three-dimensional distances to the superhit 'match point'. The average radius is then used to determine the trigger momentum by

$$p_T = \frac{r}{r_c} p_c$$

where r is the track radius of curvature, and p_c is the calibration momentum of radius r_c. The charge of the muon is determined by comparison of the sign of the circle centre parameters (x_0, z_0) with those of the calibration file.

The trigger quality is determined by the momentum resolution achieved. In Figures 11-20 and 11-21 the resolution for p_T = 20 GeV muons is shown for the barrel and end-caps, respectively, with all associated hits from GEANT processes simulated (delta-rays, bremsstrahlung, *etc.*) and random noise of 10% tube occupancy added. Note that the resolution is in the range 1.3 GeV to 1.8 GeV by Gaussian measure, but there are significant low and high-p_T tails, which will affect the sharpness of the trigger threshold.

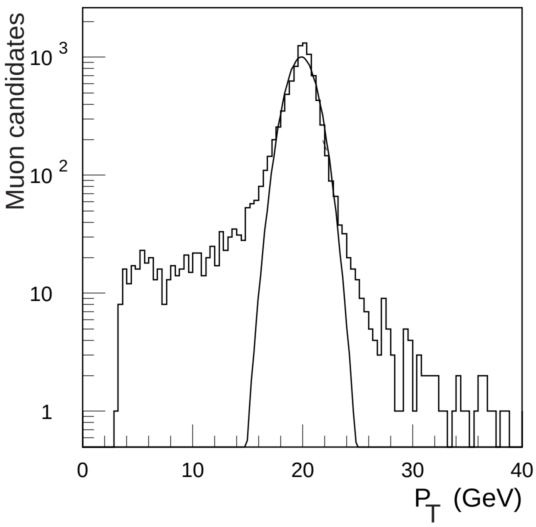

Figure 11-20 Reconstructed p_T for muons generated with p_T = 20 GeV in the barrel region $0 < |\eta| < 1$. A random noise of 10% was added.

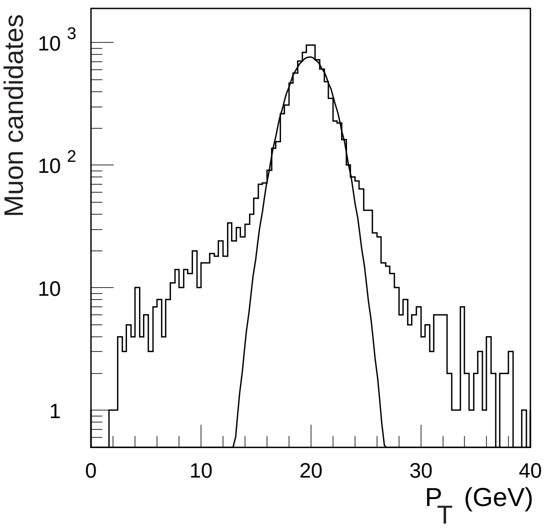

Figure 11-21 Reconstructed p_T for muons generated with p_T = 20 GeV in the end-cap region $1 < |\eta| < 2$. A random noise of 10% was added.

Figures 11-22 and 11-23 show the corresponding performance for p_T = 6 GeV muons for the barrel and end-cap regions, respectively. As expected, the resolution performance at 6 GeV is degraded from 20 GeV by the energy-loss fluctuations and multiple-scattering effects. At p_T = 6 GeV the resolution is typically about 10% by Gaussian measure; here the non-Gaussian tail is mostly on the high side of the peak. In all these figures, no regions were masked so the resolution is an indicator of the average performance over $0 < \phi < \pi/2$, $0 < |\eta| < 1$ for the barrel, and $0 < \phi < \pi/2$, $1 < |\eta| < 2$ for the end-cap.

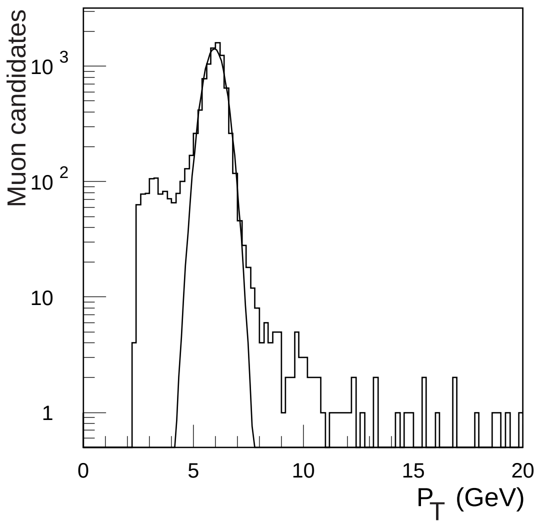

Figure 11-22 Reconstructed p_T for muons generated with p_T = 6 GeV in the barrel region 0 < |η| < 1. A random noise of 10% was added.

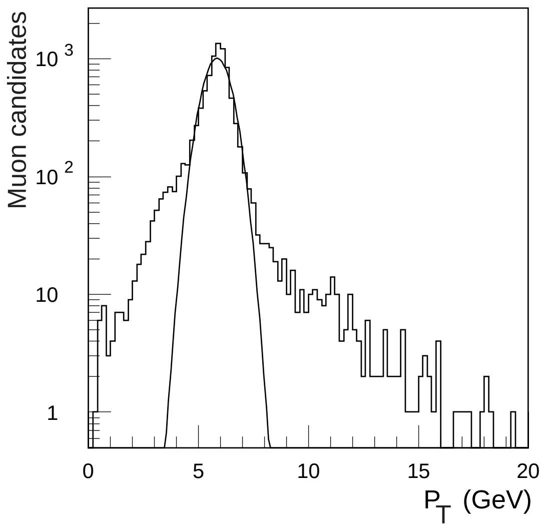

Figure 11-23 Reconstructed p_T for muons generated with p_T = 6 GeV in the end-cap region 1 < |η| < 2. A random noise of 10% was added.

Table 11-9 gives a summary of the performance for p_T = 20 GeV and 6 GeV muons. In the table the efficiency is computed for any reconstruction of the trigger momentum independent of the resultant value and the estimated error; resolutions are computed within the limits of the plots (Figures 11-20 to 11-23). The threshold curves are shown in Figures 11-24 to 11-27 for the barrel and end-cap, and low and high thresholds, respectively. The LVL1 efficiency is not included, which should further suppress the low-p_T events. The efficiency is greater than 95% in the barrel. For triggers in the end-cap it is necessary to apply track-quality cuts to achieve good threshold resolution. Regions where there is negligible bending inevitably degrade the trigger resolution. These regions ($|\eta| = 1.6 \pm 0.1$, $\phi = 0.4 + m\times\pi/4 \pm 0.1$, where m = 0, 1, 2 ...) are therefore masked. For the 6 GeV trigger in the end-cap a χ^2 cut, which requires a good circle fit, was applied. This introduces some loss of plateau efficiency, but the overall trigger threshold is much sharper than with no quality cut.

Table 11-9 Summary of reconstruction-efficiency and resolution performance.

p_T (GeV)	Detector region	Efficiency	rms resolution (GeV)	Gaussian resolution (GeV)
20	barrel	99.4 ± 0.1	3.1	1.3
20	end-cap	99.1 ± 0.2	3.1	1.8
6	barrel	99.0 ± 0.4	1.0	0.44
6	end-cap	97.2 ± 0.7	1.3	0.60

The muon spectrum (see Figures 2-3 and 2-4 in [11-1]) is approximately flat in η, and its p_T dependence can be parametrised as

$$\frac{d\sigma}{dp_T d\eta} = \frac{4.4\times10^3}{p_T^{4.7}}\frac{\mu b}{\mathrm{GeV}}$$

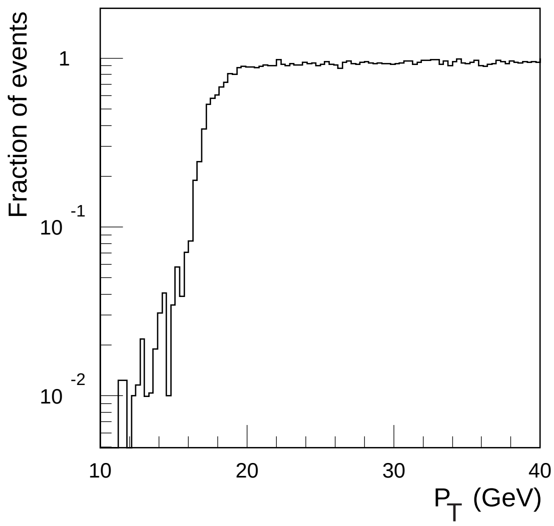

Figure 11-24 Fraction of events that pass the fixed high-p_T LVL2 threshold as function of the generated p_T for the barrel region $0 < |\eta| < 1$. A random noise of 10% was added.

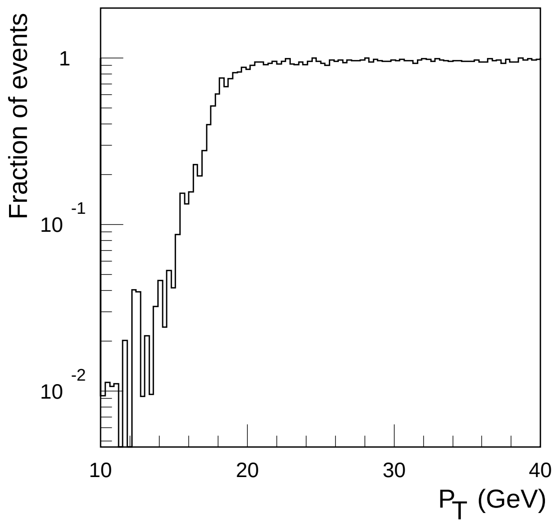

Figure 11-25 As Figure 11-24, but for the end-cap region $1 < |\eta| < 2$.

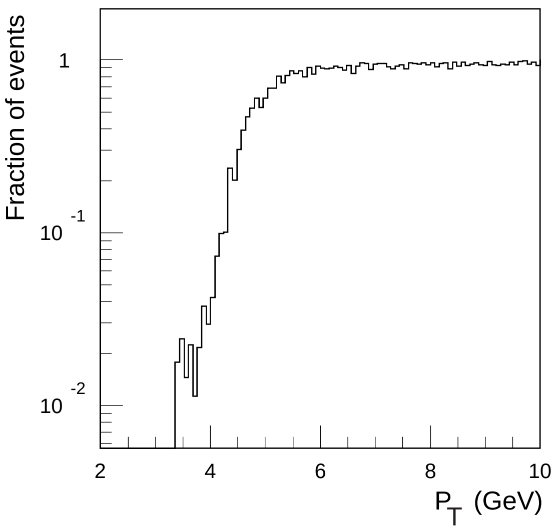

Figure 11-26 Fraction of events that pass the 6 GeV low-p_T LVL2 threshold as function of the generated p_T in the barrel region $0 < |\eta| < 1$. A random noise of 10% was added.

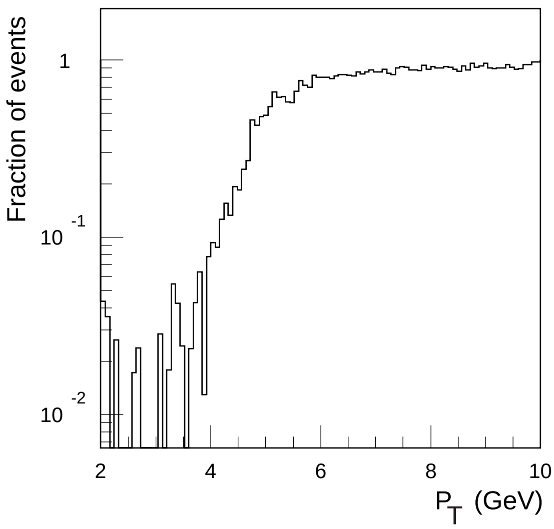

Figure 11-27 As Figure 11-26, but for the end-cap region $1 < |\eta| < 2$. A track-quality cut was imposed in addition.

where p_T is the transverse momentum in GeV at the interaction point. Convolving this spectrum with the efficiency curves, the trigger rates listed in Table 11-10 were deduced for an efficiency (plateau) of 90%.

The rates can be further reduced using information from the Inner Detector. These studies were made for the full reconstruction, but not yet for the trigger algorithms (see Chapter 8).

Table 11-10 LVL2 muon trigger rates for barrel and end-cap system and low and high luminosity thresholds. The rate obtained without quality cuts is indicated in brackets (end-cap, low luminosity). A random noise of 10% is assumed in all cases.

Luminosity	Detector region	Threshold (actual)	Rate (kHz)
low (6 GeV)	barrel	4.6 GeV	3.5
	end-cap	4.7 GeV	2.4 (5.3)
high (20 GeV)	barrel	17.5 GeV	0.29
	end-cap	17.5 GeV	0.30

11.4.2.2 Muon isolation

Muons from π/K decays or c and b semileptonic decays tend to be within jets, whereas muons from heavy objects such as W tend to be isolated. Isolation is therefore relevant for the high-p_T muon trigger and was studied using a sample of fully simulated $W \to \mu\nu$ signal events (muon p_T > 24 GeV), and $b\bar{b} \to \mu X$ background events (muon p_T > 20 GeV) (see Section 9.1 of [11-1] and [11-16]).

The best results were obtained at both low and high luminosity using information from only the EM Calorimeter. The efficiencies are summarised in Table 11-11. As an example of the selection efficiencies that one might expect, these results are weighted by the muon p_T spectrum from W and $b\bar{b}$ decays for p_T > 24 GeV. The results are given in Table 11-12. Note that only the error arising from the statistical uncertainty on the efficiencies is included.

Table 11-11 Signal and background efficiencies, in bins of muon transverse momentum, for a selection based on ECAL information at low and high luminosity. Errors are statistical.

	Low luminosity		High luminosity	
Muon p_T bin	Efficiency (%)		Efficiency (%)	
(GeV)	$W \to \mu\nu$	$b\bar{b} \to \mu X$	$W \to \mu\nu$	$b\bar{b} \to \mu X$
24–30	94.6 ± 2.1	10.4 ± 2.2	67.9 ± 4.4	9.7 ± 2.1
30–40	98.2 ± 1.0	8.2 ± 1.8	94.1 ± 1.8	10.8 ± 2.0
40– 50	97.8 ± 1.3	7.6 ± 3.3	96.3 ± 1.6	4.5 ± 2.6
> 50	99.1 ± 0.6	10.6 ± 3.3	98.2 ± 0.9	9.4 ± 3.2

Table 11-12 Example of the selection efficiencies for muonic W and $b\bar{b}$ decays, for transverse momenta greater than 24 GeV. Errors arise from the statistical uncertainty on the selection efficiencies.

Process	Low luminosity eff. (%)	High luminosity eff. (%)
$W \to \mu\nu$	97.8 ± 1.1	91.4 ± 1.9
$b\bar{b} \to \mu X$	9.6 ± 2.3	9.6 ± 2.2

11.4.3 Electron and photon trigger

Before photon and electron trigger objects can be identified, the full-granularity information from the electromagnetic and hadronic calorimeters must be used in selecting electromagnetic clusters. The LVL2 electron selection uses additionally information from the TRT and precision tracker (SCT plus pixel system). The parameters of the reconstructed features are compared, and, if consistent, are combined into electron trigger objects.

A common e/γ selection is first made by examining the cluster shower shapes and the E_T deposition in the calorimeters. The next step consists of selecting clusters likely to be due to an isolated electron or photon. The electron hypothesis is accepted if, after examining the TRT and precision tracker within the RoI, the presence of a matching charged-particle track is confirmed. Photon objects are identified by a more detailed analysis of the calorimeter shower shapes. Since the photon trigger does not use the tracking information to identify photon conversions, some clusters will be selected as both an electron and a photon. For photons higher E_T-cuts are applied than for electrons. The identification of photon and electron objects, after all LVL2 cuts, gives a total rejection with respect to LVL1 of 100 (70) for electrons and 75 (50) for photons at low (high) luminosity.

In the following sections a summary of the common e/γ selection, and the photon and electron selections is given and performance results are presented. More details can be found in Refs. [11-17], [11-18] and [11-19].

11.4.3.1 The e/γ selection

This LVL2 e/γ selection takes as input the RoIs selected by the LVL1 EM trigger, see Section 11.3.2.1, and refines the cluster energy and position measurements by using the full calorimeter granularity and an improved energy calibration. This information is then used to build shower-shape variables, which together with the transverse energy, discriminate electrons and photons from jets which passed the LVL1 EM trigger selection.

The trigger quantities used for the e/γ selection are as follows (see Section 8.2.2.4 of [11-1]).

- The transverse energy E_T calculated using the energies of all the electromagnetic-calorimeter layers in a $\Delta\eta\times\Delta\phi = 3\times7$ standard cell area within the LVL1 RoI (standard cells cover an area of $\Delta\eta\times\Delta\phi \sim 0.025\times0.025$).
- The hadronic transverse energy E_T^{had} within the LVL1 RoI.
- The ratio $R_{37} = E_{37}/E_{77}$, of energy contained in a $\Delta\eta\times\Delta\phi = 3\times7$ window to that in a 7×7 window in the second sampling of the EM Calorimeter.
- The fractional difference in energy between the strip with the maximum energy E_1, and the second maximum E_2, in the first sampling of the EM Calorimeter. The fraction is calculated as $R_\eta^{strip} = (E_1 - E_2)/(E_1 + E_2)$. Figure 11-28 shows the different structure seen in the first calorimeter sampling for electrons and jets. The trigger quantity R_η^{strip} is shown in Figure 11-29.

The quantities discussed above were chosen such that they are relatively uncorrelated and simple to implement. The dependence of the quantities on $|\eta|$ and p_T is taken into account in the implementation of the selection cuts. More details can be found in Section 8.2.2.4 of [11-1]. The values of the cuts were optimised so as to give an efficiency of ~95% for 20 (30) GeV p_T electrons passing the LVL1 selection at low (high) luminosity. The corresponding values of the E_T cuts

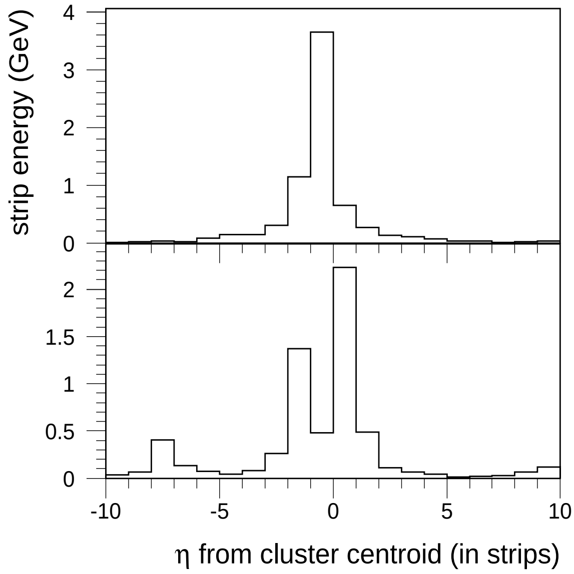

Figure 11-28 Distribution of the signals in η-strips of the first EM Calorimeter sampling for a 30 GeV electron (top) and a jet (bottom). The distributions are centred at the cluster position. The events are chosen to show the typical features after the LVL1 trigger selection at high luminosity.

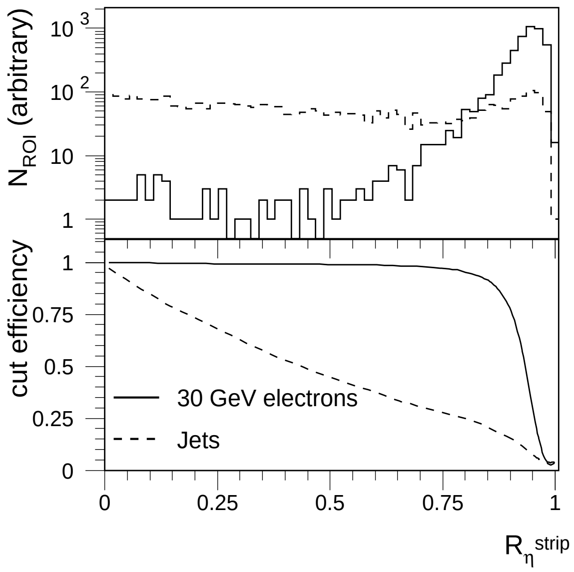

Figure 11-29 Distribution of number of RoIs accepted (top) as function of R_η^{strip} for E_T = 30 GeV electrons and jets at high luminosity. Efficiency as a function of a cut on R_η^{strip} (bottom). The distributions are given after the LVL1 trigger selection. No other cuts have been applied.

Table 11-13 Overall cumulative efficiencies of LVL1 and LVL2 *e/γ* selection for single p_T = 20 GeV electrons at low luminosity, and for single p_T = 30 GeV electrons at high luminosity. The corresponding trigger rates are also shown.

	Low luminosity		High Luminosity	
Selection requirements	Efficiency (%)	Rate (kHz)	Efficiency (%)	Rate (kHz)
LVL1 CALO	95	7.9	95	25.1
E_T^{em}	93	5.6	94	16.3
E_T^{had}	93	4.1	94	11.6
R_{37}	92	2.3	94	8.5
R_η^{strip}	91	1.0	92	3.9

were 16 GeV (25.5 GeV) for the nominal 20 GeV (30 GeV) thresholds used at low (high) luminosity. The values of the other cuts are listed in Section 8.2.2.5 of [11-1]. With these cuts a rejection of 7.6 (6.4) with respect to the output of the LVL1 trigger for low (high) luminosity is obtained. Table 11-13 shows the efficiencies and rates for the e/γ selection after each step of the selection requirements is applied.

11.4.3.2 The photon trigger

An acceptable photon trigger rate is achieved by applying tighter cuts than in the e/γ selection and by using additional quantities to further reject π^0s and jets [11-19]. Only calorimeter information is used. The additional trigger quantities used to select LVL2 trigger photon objects are:

the energy-weighted shower width in the η-direction, $\omega_\eta = \sqrt{\langle\eta^2\rangle - \langle\eta\rangle^2}$, in the second sampling of the EM Calorimeter, calculated in a $\Delta\eta\times\Delta\phi = 3\times5$ cell window, and the shower shape in the first sampling, R_η^{shape}. This quantity measures the fraction of energy outside the shower core and is calculated from $R_\eta^{shape} = (E_7 - E_3)/E_3$, where E_7 and E_3 are the energies in 7 and 3 strips respectively around the cluster centroid.

Using these quantities, the photon trigger selection is optimised such that converted and unconverted photons have a similar selection efficiency. A more sophisticated analysis using the calorimeter and the Inner Detector information (*e.g.* at the Event Filter or offline level) can reject or select these photons at a later stage, see Chapter 7.

The rates from jets as a function of the sequential LVL2 trigger cuts are shown in Figure 11-30 and Figure 11-31. At low luminosity, raising the E_T threshold by 9 GeV reduces the background rate by a factor of two. At high luminosity, this rate reduction is achieved with a threshold increase of 15 GeV for the single-object trigger. In case the background rate is too high for the double-object trigger at high luminosity, the rate can be reduced by raising the E_T threshold of the second object. This hardly affects the efficiency for $H \rightarrow \gamma\gamma$ events, which is the most important physics process requiring photon identification, see Chapter 19.

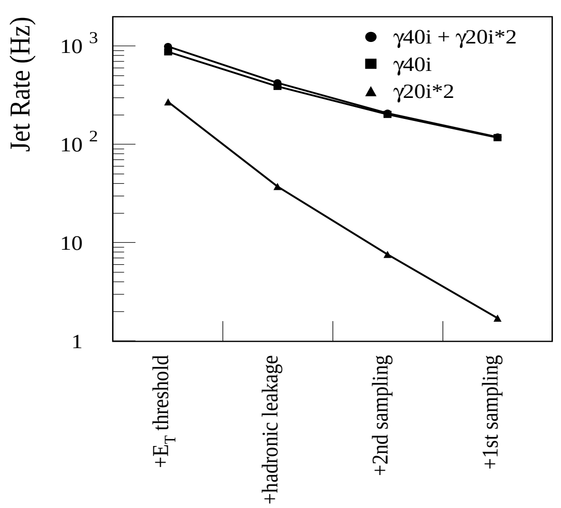

Figure 11-30 Rates from jets at low luminosity for the different LVL2 trigger menu items as a function of the LVL2 trigger cuts in the different parts of the calorimeter. The cuts are applied consecutively and in addition to the LVL1 selection.

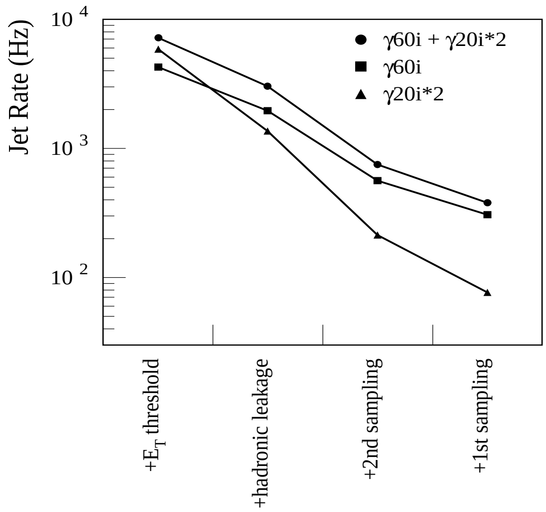

Figure 11-31 As Figure 11-30, but for high luminosity.

Table 11-14 summarises the photon efficiencies at various transverse energies and the corresponding background rates for low and high luminosity. The table also shows the expected efficiencies at low and high luminosities for selecting di-photon final state Higgs events with $m_H = 100$ GeV with the various trigger menu elements. The table includes the photon trigger menu items as defined in Section 11.7.2 and [11-27], *e.g.* γ40i is a trigger for isolated photons of $E_T > 40$ GeV.

Table 11-14 Expected efficiencies at threshold and background rates for the LVL2 photon trigger at low and high luminosity. The trigger efficiency for $H \to \gamma\gamma$ events is also shown for m_H = 100 GeV.

Trigger	luminosity	photon efficiency (%)	Higgs efficiency (%)	LVL2 Rate (Hz)
γ40i	low	95.5 ± 0.3	98.3 ± 0.2	117 ± 10
γ20i $\times$ 2	low	81.8 ± 0.4	92.6 ± 0.2	2 ± 1
γ40i OR γ20i $\times$ 2	low		98.3 ± 0.2	119 ± 10
γ60i	high	95.5 ± 0.5	55.0 ± 1.0	304 ± 48
γ20i $\times$ 2	high	81.3 ± 1.0	93.3 ± 0.5	76 ± 24
γ60i OR γ20i $\times$ 2	high		95.3 ± 0.4	380 ± 54

11.4.3.3 The electron trigger

After the LVL2 common e/γ selection described in Section 11.4.3.1 the trigger rates, calculated from the analysis of a sample of simulated di-jet events with and without pile-up, are 1 kHz at low luminosity and 3.9 kHz at high luminosity. A breakdown of the various contributions to these trigger rates is shown as the open histogram in Figure 11-32. For ~90% of events passing the calorimeter e/γ selection, the highest-E_T cluster in the event is due to photons (~60% from the decay of π^0s, the rest from η / ω decays, bremsstrahlung and prompt photons). In the majority of cases the π^0 causes an e/γ trigger because the photons are not well separated and cannot be resolved into separate clusters. In ~20% of all cases it is an electron from a photon conversion which causes the event to trigger. By searching for a track in the Inner Detector and by requiring a match between the measured track parameters and the calorimeter cluster, the trigger rate may be significantly reduced for both cases.

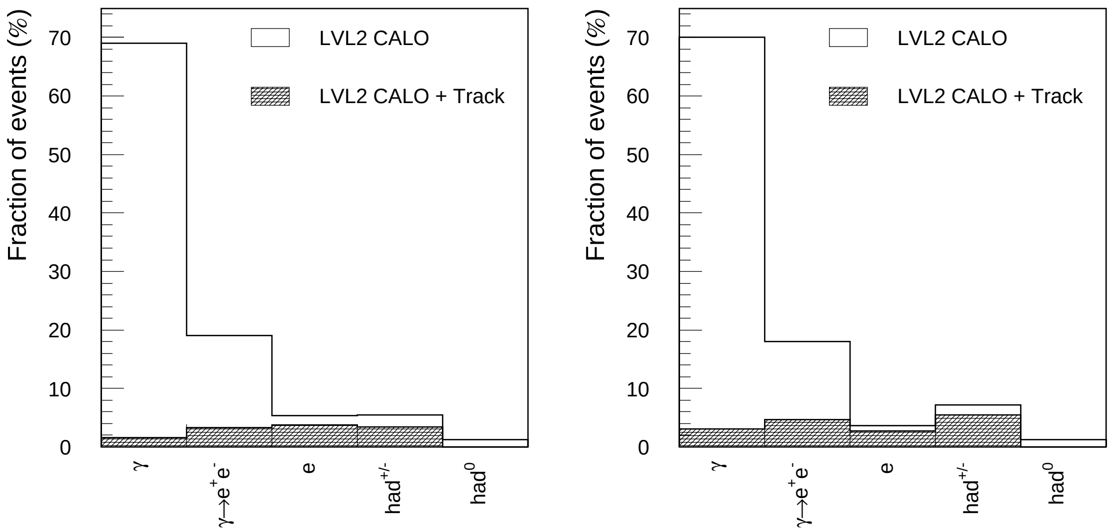

Figure 11-32 The highest p_T particle in events passing the LVL1 and LVL2 calorimeter selections (open histogram) and for those events containing, in addition, tracks in the TRT and precision tracker matched to the calorimeter cluster (hatched). The distributions are shown for jet events without pile-up (left) and with pile-up at high luminosity (right).

A search for track candidates is performed separately in the TRT and precision tracker. The same basic method is used in both cases. This consists of an initial search using a histogramming method to identify sets of hits likely to form a track, followed by a fit to each set of selected hits. In the initial search a histogram is formed of the number of hits along possible track trajectories. For all trajectories with a number of hits above some pre-defined threshold, a fit is performed. The best track candidate is chosen and returned as input to the electron-trigger decision. The TRT uses two readout thresholds. Signals passing the higher threshold are more likely to have been caused by Transition Radiation, characteristic of an electron track. The number of hits on a track passing the higher threshold can, therefore, be used to select track candidates likely to be due to an electron. Details of the algorithms and the process by which the best candidate is selected can be found in References [11-20] and [11-1].

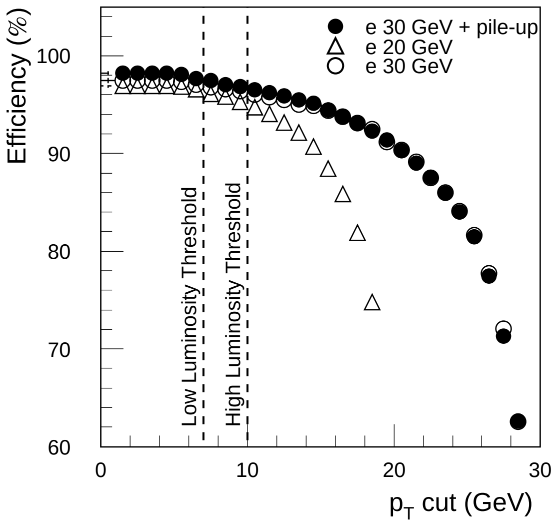

Figure 11-33 Efficiency of the precision tracker as a function of the p_T cut value (GeV) for single-electron events passing the LVL1 and LVL2 calorimeter selection.

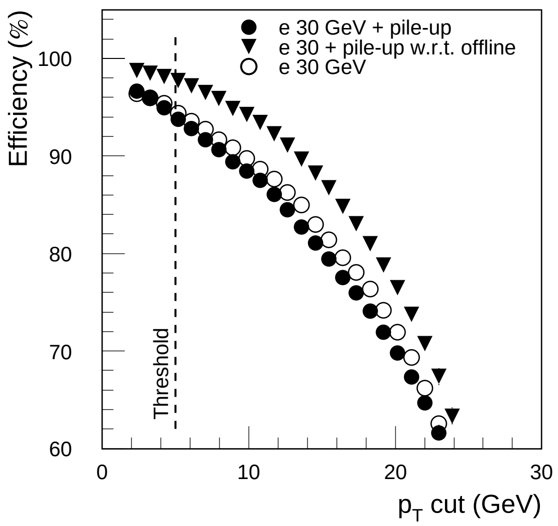

Figure 11-34 Efficiency of the TRT algorithm as a function of p_T cut (GeV). The efficiency is shown relative to events passing the LVL1 and LVL2 calorimeter selections (circles) and relative to those events additionally containing a track found by the offline Inner Detector pattern-recognition software (triangles).

The TRT and precision tracker each return the parameters of a single track candidate found within the LVL1 RoI. The next step in the electron trigger is to apply a p_T cut to these candidates. This discriminates against the predominately low-p_T tracks in jet events. The efficiency of the precision tracker to reconstruct tracks from 20 GeV and 30 GeV p_T electrons is shown as a function of p_T cut in Figure 11-33. Values for the p_T cut of 7 GeV (10 GeV) were chosen for low (high) luminosity respectively so as to give an efficiency of 96% for events passing the LVL2 calorimeter selection. The corresponding distributions of efficiency as a function of the p_T cut are shown for the TRT in Figure 11-34. Since a significant proportion of electrons lose a large fraction of their energy via bremsstrahlung before entering the TRT, the efficiency for reconstructing a track in the TRT rises slowly with decreasing value of the p_T cut. A p_T cut of 5 GeV was applied.

The requirement of a track in both the precision tracker and the TRT, in addition to the e/γ calorimeter selection with a nominal E_T threshold of 20 (30) GeV, gives a rejection with respect to LVL1 of 25 (50) for jets without (with) pile-up at high luminosity. The rates and efficiencies are given in Table 11-15. There is a corresponding loss of efficiency of 9% (7%) for single electrons passing the e/γ selection at low (high) luminosity. In a sizeable fraction of cases the electrons rejected have lost a significant amount of p_T via bremsstrahlung. These tracks are also likely to fail an offline selection. A fairly loose set of offline Inner Detector cuts has been defined[1], in order to measure the trigger efficiency for the sub-set of events that would pass an offline physics selection (see Table 11-15). Of the single-electron events at low or high luminosity passing both the LVL2 calorimeter and the offline selections, 96% have tracks found by the trigger algorithms in the TRT and precision tracker.

Table 11-15 Overall combined efficiencies of LVL1 and LVL2 for single p_T = 20 GeV electrons without pile-up (10^{33} cm^{-2}s^{-1}), and for single p_T = 30 GeV electrons with pile-up at high luminosity. Efficiencies are also given relative to events passing both the LVL1 and LVL2 e/γ calorimeter and offline Inner Detector selections. Trigger rates are shown at low and high luminosity determined from samples of jet events without and with pile-up. Details of the Inner Detector track cuts and offline selection are given in [11-1], Section 9.3. In addition, performance results for a tighter set of track cuts are given (bottom row).

	Low luminosity			**High Luminosity**		
Selection requirements	Effic. (%)	Rate (kHz)	Effic. wrt offline ID (%)	Effic. (%)	Rate (kHz)	Effic. wrt offline ID (%)
LVL1 + LVL2 CALO	91	1.00	–	92	3.9	–
Precision Track	87	0.20	98	89	1.4	98
TRT Track	83	0.39	97	86	1.9	97
Precision and TRT tracks	82	0.19	96	85	1.1	96
Precision track matched to CALO	87	0.14	98	88	0.7	97
TRT track matched to CALO	83	0.31	96	85	1.5	96
Precision and TRT tracks both matched to CALO	82	0.13	95	83	0.6	94
Precision and TRT tracks both matched to CALO (tighter cuts)	77	0.08	91	79	0.4	90

In the majority of jet events passing the e/γ selection, the calorimeter cluster is not caused by a single charged track and hence does not match well in position with the track extrapolated from the Inner Detector. Cuts on the separation in azimuthal angle and pseudorapidity between the extrapolated track and the cluster position thus provide good discrimination against jet events. In addition, the momentum spectrum for tracks in jet events is peaked towards low values. As a result, in jet events, the cluster energy can be much larger than the momentum of any single track. The ratio of the transverse energy of the calorimeter cluster to the p_T of the Inner Detector track, E_T/p_T, therefore provides additional discrimination against jet events. Performance measurements are given in Table 11-15 for a relatively loose set of cuts on these parameters, details of which can be found in [11-1]. With these cuts, rejections with respect to LVL1 of 60 (40) are achieved for jets at low (high) luminosity. A breakdown of the composition of these triggered events is given as the hatched histogram in Figure 11-32. A comparison with the breakdown for events after the e/γ selection alone (open histogram) shows the greatest jet rejection is obtained for clusters due to photons, where the photons do not convert. However a significant rejection is also obtained in the case of conversions.

1. The set of offline cuts used is not complete; for example no cut was applied to the ratio E_T/p_T. More details of the offline cuts are given in [11-1].

By varying cut values, some flexibility in the efficiency and rejection may be achieved. As a second example, results obtained with tighter track cuts are given in the bottom row of Table 11-15. With these cuts, rejections of 100 (70) are achieved at low (high) luminosity for an additional 4% loss of efficiency for single electrons.

The algorithms used for the work reported here have been designed to be suitable for an online implementation. Some initial benchmarking results on execution times are available. In addition, work is well advanced to benchmark the algorithms in a realistic trigger environment as part of the LVL2 trigger Pilot Project [11-4]. The work on optimising the association of the information from the Pixels, SCT, TRT and calorimeter in terms of efficiency for electrons and rejection of jet events is ongoing. More details of the programme of work are given in [11-1].

The results presented here indicate that the required trigger rates can be achieved at low and high luminosity with an efficiency of better than 90% for events that would pass an offline selection. Further improvements in the algorithms and selection cuts are being pursued. These include the use of the LVL2 calorimeter information to reduce the region of interest for the track search and the evaluation of more sophisticated but potentially slower algorithms.

11.4.4 τ/hadron trigger

The τ/hadron trigger may be used in coincidence with other triggers, such as a muon or missing-E_T trigger, to improve the efficiency for triggering or to allow the use of lower thresholds. Examples are a trigger for the $Z \to \tau\tau$ decay and the decay of the low-mass $A \to \tau\tau$.

Separation of τ/jet at LVL2 is based on calorimeter and tracking information. The calorimeter selection was described in detail in Section 8.2.3 of [11-1]. The selection based on tracks was presented in Section 9.4 of [11-1]; the preliminary results available at the time used the information of the generated tracks (assuming 90% tracking efficiency).

The signal selection was tuned using events of the type $A \to \tau\tau$ and the rejection of background from jets was optimised using QCD jet samples. The calorimeter selection was performed in two steps. The EM plus hadronic transverse energy contained in a small core of $\Delta\eta\times\Delta\phi = 0.15\times0.15$ was required to be above threshold, *e.g.* $E_T^{core}(em+h) > 50$ GeV. The fraction f_{core} of EM energy in the core was required to be greater than 85%, where the RoI region covers $\Delta\eta\times\Delta\phi = 0.4\times0.4$, $f_{core} = E_T^{core}(EM) / E_T^{RoI}(EM) > 0.85$.

Table 11-16 Rates from jets and τ efficiencies for LVL2 τ selections applied sequentially. The columns correspond to different cuts on the LVL2 core E_T. For the first column only the LVL1 cut (E_T > 30 GeV) is applied, for the remaining columns increasing cuts in core E_T are applied, which correspond to jet efficiencies of 40%, 30% and 20% (relative to LVL1). The selections are explained in the text.

	LVL1		E_T > 50 GeV		E_T > 55 GeV		E_T > 63 GeV	
Selection	**Rate Hz**	**Eff$_\tau$ %**	**Rate Hz**	**Eff$_\tau$ %**	**Rate Hz**	**Eff$_\tau$ %**	**Rate Hz**	**Eff$_\tau$ %**
E_T^{core}	3110	100.0	966	78.0	719	71.8	418	62.2
+ f_{core} (EM) > 0.85	1090	87.0	316	70.6	245	65.2	158	57.0
+ $1 \le N_{trk} \le 3$	670	75.2	158	59.7	110	54.7	63	47.3
+ $N_{trk} = 1$	250	42.9	45	33.3	30	30.2	12	26.7

Table 11-16 shows the evolution of the τ efficiencies and the rates from jets, when these selections are applied. The E_T cut reduces the LVL1 τ trigger rates by a factor of three, and the requirement on core energy fraction gives an additional reduction of more than a factor three, while keeping the τ efficiency close to 70%. Further rejection is obtained by restricting the number N_{trk} of charged tracks associated to the τ RoI, *e.g.* for a threshold of $p_T > 2$ GeV. $1 \leq N_{trk} \leq 3$.

The resulting trigger rate is 160 Hz, and the τ efficiency is close to 60%. Further jet rejection could be obtained by requiring exactly one track; in this case the τ efficiency is reduced to ~30% for one-prong decays.

11.4.5 Jet trigger

The aim of treating jets at LVL2 is to reduce the rate of events containing jets by improving the measurement of the energy and position of the jets. The improvement in the jet measurement is achieved by a refined energy calibration, a jet definition and threshold adjustments. The aim is to achieve an efficiency of 95% with respect to the LVL1 jet, or 90% with respect to the reference jet.

An example of a LVL2 jet algorithm is described in Section 8.2.4 of [11-1]. For a given LVL1 RoI, a window around the RoI direction with a size of 1.0×1.0 was selected. The energy depositions are first summed up into towers of $\Delta\eta\times\Delta\phi = 0.1\times0.1$, applying calibrations and thresholds per cell. A threshold per cell is of great importance due to the large number of cells involved. Then a cone algorithm (with radius $R = 0.4$ and E_T threshold on the seed cell of 1 GeV) was run on the trigger towers inside this window. The reference jet was defined with the same algorithm, but using the generated particles before detector simulation (excluding neutrinos and muons and using only particles with $|\eta| < 3.2$).

The achieved (Gaussian) position resolution is $\Delta\eta \sim \Delta\phi \sim 0.03$, but there are significant non-Gaussian tails. The distance $\Delta R = (\Delta\eta^2 + \Delta\phi^2)^{1/2}$ between the reconstructed and the reference jet in the (η, ϕ) plane has a mean of about 0.036, which is an improvement compared to the LVL1 resolution of about 0.2×0.2 described in the Section 11.3.2. This improvement in spatial resolution is important for the separation of nearby jets and the possible calculation of invariant masses of jets. The improved energy measurement allows sharper thresholds, which in turn reduces the rate of accepted events.

Figure 11-35 shows for the case of low luminosity (10^{33} cm^{-2}s^{-1}) the rates for events at LVL2 with at least n jets, where n = 1 to 4. Due to the particle-level filter applied to the data sample used here, it has to be kept in mind that the rate for single inclusive jets is biased. The rate shown can only be taken as a lower limit.

The ratio of the LVL1 and LVL2 rates is displayed in Figure 11-36 as a function of the nominal jet E_T for events with $N_{jet} \geq 1$ to $N_{jet} \geq$ 4jets. One observes a decrease of the ratio with increasing jet energy, indicating that the effect of the 1 GeV threshold per trigger tower at LVL1 becomes less important at larger jet energies. The ratio has a value of about two at a nominal jet energy of 80 GeV for all jet classes. At larger nominal energies, the factor slowly approaches a value close to one. For smaller energies down to 50 GeV the ratio is larger, giving factors between four and six at 50 GeV.

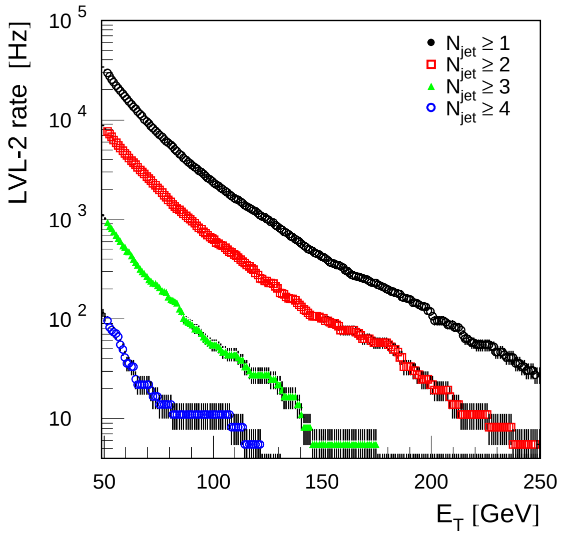

Figure 11-35 Rates for inclusive jet and multi-jet production at low luminosity (10^{33} $cm^{-2}s^{-1}$) without taking into account the effect of pile-up. The rates shown are given for 90% efficiency of the LVL2 algorithm with respect to the reference jet, see text. Due to the particle-level filter applied to the simulation used, the inclusive single jet rate is underestimated.

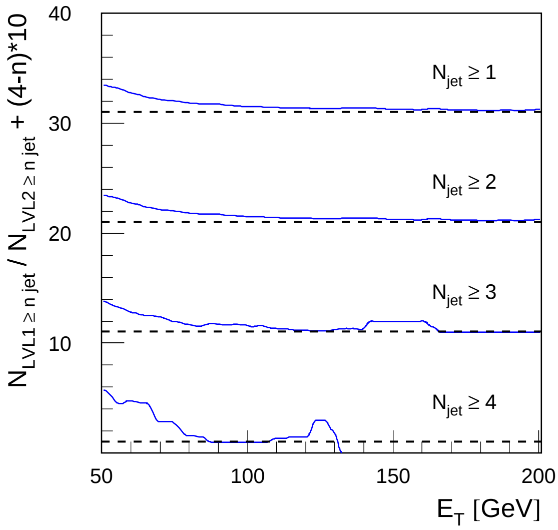

Figure 11-36 Ratio of the rates for inclusive jet and multi-jet production at LVL1 with respect to LVL2, shown for low luminosity (10^{33} $cm^{-2}s^{-1}$) without taking into account the effect of pile-up. The ratios shown correspond to 90% efficiency for LVL2 and 95% efficiency for LVL1 with respect to the reference jet, see text. For each ratio an offset of $(4 - n)\times10$ for $\geq$ n jets is added. The dashed line indicates a value of 1 for the ratio.

11.4.6 Tagging of *b*-jets at LVL2

The possibility of implementing a LVL2 *b*-jet tag trigger based on impact-parameter information is under study. Issues to be addressed include the feasibility (beam-position stability, alignment, *etc.*) and comparing the merits of making the selection at LVL2 or in the Event Filter where more complex algorithms and better alignment constants might be available. No strong physics case for this trigger has been established [11-22], but it would add to the flexibility of the trigger.

An algorithm for finding tracks in the barrel pixel detector was studied and presented in [11-1]. Due to the *b*-quark lifetime there is clear distinction between the reconstructed transverse impact parameters (d_0) for *b*- and *u*-quark jets. A simple *b*-tagging algorithm using a likelihood method has been used to distinguish between the different jet types. The performance of this algorithm is illustrated in Figure 11-37, which shows the *u*-quark-jet rejection as a function of the *b*-tagging efficiency for simulated *WH* events ($H \to b\bar{b}$) without and with pile-up for a Higgs mass of 400 GeV. A rejection factor of 20 can be achieved for a *b*-tagging efficiency of 50% in the presence of pile-up at high luminosity. It should be noted that WH events are triggered by the $W \to e\nu / \mu\nu$ decay, and no *b*-tag is required at the trigger level for this channel.

The trigger and the offline *b*-tagging algorithm (using the xKalman reconstruction program with standard analysis cuts – see Chapter 10) have been compared in order to check their correlation. The two methods have been applied to the same sample of 400 GeV Higgs events. It was found that the correlation between the weights generated by the two methods is sufficient to avoid an excessive degradation of the pure offline performance. To study this further, a trigger

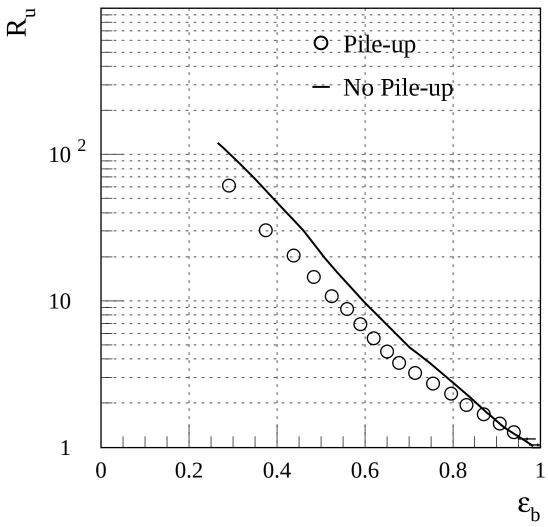

Figure 11-37 *u*-jet rejection as a function of *b*-jet efficiency for 400 GeV Higgs at high luminosity compared to low luminosity in the barrel.

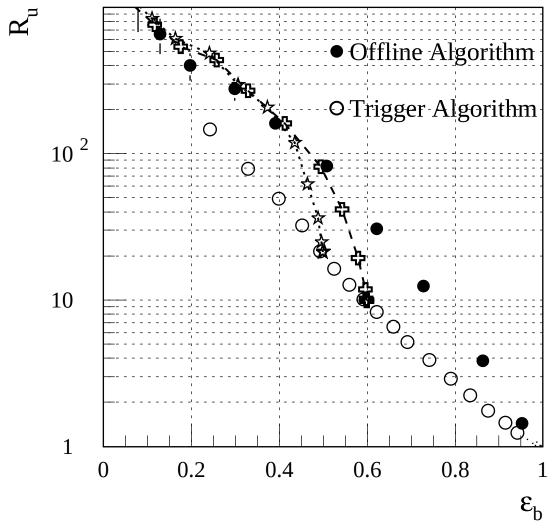

Figure 11-38 *u*-jet rejection as a function of *b*-jet efficiency for 400 GeV Higgs at low luminosity in the barrel for the trigger and offline algorithms. The lines show the offline performance starting from different trigger preselections (stars: $R_u = 10$, crosses: $R_u = 20$).

selection corresponding to $R_u = 10$ (20) and $\varepsilon_b = 60\%$ (50%) has been applied. To this LVL2 trigger selection, offline cuts (corresponding to different ε_b) were applied in order to see whether the pure offline performance could be restored. The results are shown in Figure 11-38. The offline performance is recovered after an offline cut corresponding to a final *b*-tagging efficiency of around $\varepsilon_b = 45\%$ (40%). Further, it can be seen that the same rejection ($R_u \approx 90$) as would be achieved in the absence of any trigger cuts and with $\varepsilon_b = 50\%$ can be obtained with a corresponding loss of *b*-tagging efficiency of about 2% (5%).

It remains to be seen whether improvements in the trigger performance and increased overlap with the offline algorithms can be achieved, and whether more realistic conditions (misalignments, uncertainties in the beam-spot position, degradations in silicon efficiency) would significantly degrade the performance quoted here.

11.5 Missing E_T and total scalar E_T

All calorimeter data have to be transferred to LVL2 for recalculating E_T^{miss} and total scalar E_T. The associated data traffic is of concern. Improvements of E_T^{miss} are however possible without recalculation – *e.g.* the LVL1 E_T^{miss} vector can be corrected for the p_T missed due to energetic muons and for LVL1 ADC saturation. The E_T^{miss} trigger will be used together with other signatures, such as leptons and jets. Events with very large missing-E_T may also indicate new physics.

11.6 Triggers for *B*-physics channels

11.6.1 Introduction and overview

At the LHC the *b*-quark production cross-section is many orders of magnitude higher than for e^+e^- machines and their dedicated *B*-physics experiments. For centrally produced *b*-quarks with $b \to \mu$ ($p_T^\mu > 6$ GeV) within the acceptance of the ATLAS detector, the Monte Carlo generator PYTHIA predicts a cross-section of ~2.4 μb. The azimuthal angle between the produced *b*-quark and $\bar{b}$-quark extends over the full range of 0–2π. The high particle-multiplicity in *b*-quark events, combined with a typical pile-up of 2.3 minimum-bias events per bunch crossing, at low luminosity of 10^{33} cm^{-2}s^{-1}, gives rise to a large combinatorial background (for reconstructing *B*-hadron decays), which must be rejected at the trigger level.

The *B*-physics programme is discussed in Chapter 17; the *B*-physics trigger has been previously described in [11-1]. All studies, except those of the *B* production mechanism, are based on the reconstruction of exclusive *B*-hadron decays, and in many cases also on the partial identification of the accompanying (anti-) *B*-hadron in order to tag the flavour of the *B*-hadron at production.

The physics channels currently studied may be grouped as follows (see Table 10-1 in [11-1]).

- Hadronic channels, tagged by the decay $b \to \mu$ of the accompanying *B*-hadron. The hadrons are required to have transverse momentum $p_T > 1.5$ GeV for decays with high multiplicity (*e.g.* $B_s \to D_s\, \pi$) or $p_T > 4$ GeV for decays with low multiplicity (*e.g.* $B_d \to \pi\pi$).
- *B* decays to J/ψ with subsequent decay $J/\psi \to \mu\mu$ or $J/\psi \to ee$. Tagging may be provided either by the semi-leptonic decay of the accompanying *B*-hadron, by *B*–π correlation or jet-charge measurements.
- Final states with very small branching fractions and containing muons (*e.g.* $B \to \mu\mu$, $B \to K^{*0}\mu\mu$).

The key selection criteria at the analysis level are based on particle identification (μ / *e* / hadrons), mass and vertexing cuts. The LVL2 trigger may make use of all these selections, although the use of vertexing or impact-parameter criteria is still under investigation and was not applied in the studies presented here.

The LVL1 trigger selects *b*-events through the muon from the decay of one of the *B*-particles, with $p_T^\mu > 6$ GeV. The LVL2 trigger confirms the trigger muon first in the muon spectrometer and subsequently in the Inner Detector. At this stage the threshold is sharpened and the contribution from π/*K* decays may be reduced. The muon from the decay of a *B*-particle does not indicate the direction of flight of the other *B*-hadron. For further selections, an unguided track search is therefore necessary; this can be achieved by a track search in the full TRT. The TRT tracks are then used as seeds for the track search in the precision tracker. The resulting three-dimensional tracks may be required to originate close to the trigger muon production vertex, thus rejecting tracks from additional minimum-bias events with primary vertices displaced in the *z*-coordinate. Three-dimensional information is also needed for mass cuts and for extrapolation to the calorimeter and Muon Systems to identify additional soft muons and electrons.

The LVL2 trigger addresses specific channels semi-exclusively. The signal is usually only a small fraction of the accepted rate. For example, in events selected with $J/\psi \to ee$ the rate is dominated by misidentified hadrons and conversion electrons. Similarly, the D_s and $B \to \pi\pi$ triggers are dominated by combinatorial backgrounds. The di-muon rate is dominated by muons from decays of B-hadrons and from decays in flight of charged pions and kaons. The contributions from charm and direct J/ψ production are minor.

Impact-parameter cuts may be applied at LVL2 or in the Event Filter. The use of the precise information from the pixel detector at an early stage of the LVL2 decision chain is currently under study. Secondary-vertex finding can reduce the backgrounds in the offline analysis.

11.6.2 Tools and algorithms for *B*-physics trigger studies

The tools used for B-physics studies are described in detail in [11-1], Section 10.2. In this section, only a short account and update on the algorithms and key selections are given.

11.6.2.1 Tracking in the Inner Detector

The trigger algorithms for tracking in the Inner Detector are similar to those used for the RoI-guided LVL2 tracking trigger, but they must be efficient for much lower thresholds; no RoI guidance is available for the TRT algorithm. Typical p_T thresholds are 1.5 GeV for hadron and 0.5 GeV for electron candidates. Fast histogramming methods are used for the track search in the TRT and in the precision tracker. A description of the algorithm steps is given in Refs. [11-1] and [11-23], together with the resolutions achieved for single particles of fixed p_T. For the measurement of execution times, efficiency, fake-track rate, and electron-identification power, fully-simulated events with $B_d^0 \to J/\psi(ee)\, K_s^0$ decays with pile-up were used.

Figures 11-39 and 11-40 show the track-finding efficiency for the TRT algorithm as functions of the generated p_T and η for $B \to \mu X$ with pile-up added for low-luminosity operation.

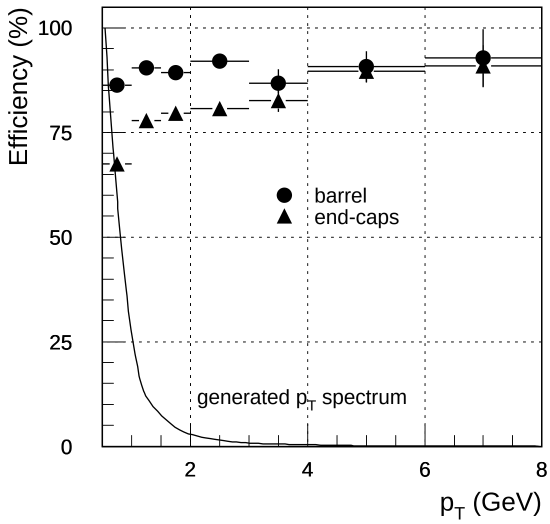

Figure 11-39 Track-reconstruction efficiency for pions with p_T > 1 GeV, integrated over $|\eta|$ < 0.8 for the barrel and 0.8 < $|\eta|$ < 2.5 for the end-cap, versus generated p_T. The inlay shows the p_T spectrum of all pions in this η and p_T range.

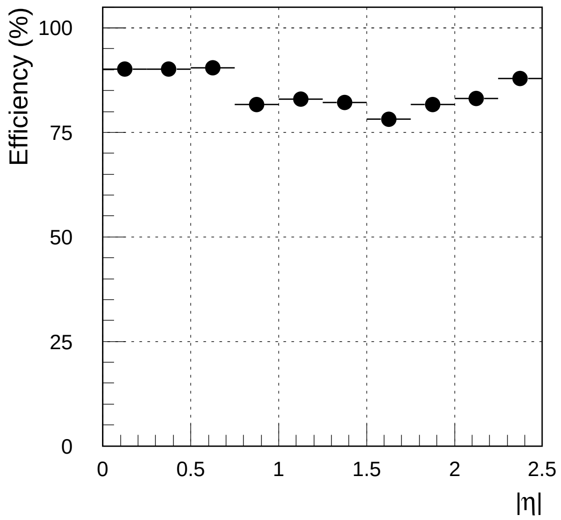

Figure 11-40 Track reconstruction efficiency for pions, integrated over generated p_T > 1.0 GeV, versus generated $|\eta|$.

A Kalman filter algorithm [11-24] is presently being studied as a possible alternative trigger algorithm for the precision tracker. The TRT track segments are extrapolated into the SCT. Trajectories within the initial road which contain a sufficient number of hits are retained. Most studies of specific *B*-physics channels were performed with a modified version of the ATLAS offline Kalman filter (xKalman [11-25]), which was adapted for trigger studies. The resulting rates for the different *B*-physics channels are summarised in Section 11.6.3.

All TRT algorithms perform the initial track search without making use of the drift time. Because of the low p_T of the *B* decay products, sufficient momentum resolution can be achieved using only the position of hit straws in the track fit. The studies assume, however, a constant magnetic field of 2 T over the whole tracker volume. The effect of the realistic solenoidal field was studied in [11-26]. Modifications to the TRT algorithms will be needed in the end-cap regions, *e.g.* for $|\eta| > 2$, where the magnetic field drops to 0.6 T.

11.6.2.2 Soft-electron identification

The efficient and clean identification of low-p_T electrons is an important element for *B*-physics triggers. This can be achieved using the combination of the Inner Detector, including the transition-radiation signature in the TRT, and the fine-grained EM Calorimeter. Electron-candidate tracks are extrapolated to the different longitudinal samplings of the EM calorimeter. A cluster of calorimeter cells is formed around each impact point and is used to measure the cluster energy as well as the longitudinal and transverse shape of the cluster. Depending on the set of selections, efficiencies of 80% to 65% are achieved for $b\bar{b} \to \mu e X$ events, where $p_T^{\mu} \geq 6$ GeV and $p_T^{e} \geq 5$ GeV; the corresponding efficiency for background events (excluding electrons from *b* or *c* quarks) is between 3% and 0.2%. The efficiency for this background is ~17% if only the TR function is used, requiring the fraction of transition radiation hits to exceed 0.14. More details are given in Section 10.2.3 of [11-1] and in Chapter 17.

11.6.2.3 Soft-muon identification

The LVL2 trigger for *B*-physics includes a selection on di-muons, with $p_T > 6$ GeV for the first muon, and a lower threshold for the second muon, normally 5 GeV, but thresholds as low as 3 GeV were studied as well. Two methods have been considered for identifying the lower-p_T muons.

- The muon spectrometer may be used if the muon has sufficient momentum to reach it; this is the case for $p_T > 5$ GeV muons in the barrel, and for $p_T > 3$ GeV in the end-caps.
- The identification of muons of 3 GeV $< p_T <$ 7 GeV in the barrel, using the energy deposition in the last two layers of the Tile Calorimeter.

Results are reported in [11-1], Section 10.2.4. The muon identification in the Tile Calorimeter can reach high efficiencies > 90% for $p_T > 3$ GeV muons in the region of $|\eta|$ from 0.1 to 0.6 (barrel) and 0.9 to 1.2 (extended barrel). The pion rejection factors are p_T and η dependent and have typical values of 10 to 50, for momenta from 3 to 5 GeV, respectively. The most recent results for offline reconstruction are reported in Chapter 8 and [11-12].

11.6.3 Summary of *B*-physics rates

The rates for *B*-physics channels expected after the LVL1 and LVL2 triggers are summarised in Tables 11-17 and 11-18. Most of the events accepted by LVL1 have a muon with true p_T lower than the nominal 6 GeV threshold, and originate mainly from π/K decays. The rate is reduced to 9000 Hz by requiring that the muon is reconstructed in the Inner Detector with $p_T > 5.9$ GeV. Possible further rejection of $\pi/K \to \mu\nu$ decays by requiring matching of the Inner Detector and muon-spectrometer tracks is under investigation (Chapter 8). The selection of specific *B*-physics channels was discussed in Section 10.3 of [11-1]. Some of the selection criteria are indicated in the summary Table 11-18, and details are described in Section 10.3.3 of [11-1].

Table 11-17 Summary of *B*-physics trigger: rate of events with one muon with p_T threshold 6 GeV after LVL1 and after confirmation at LVL2, represented here by Inner Detector reconstruction only.

	Trigger requirement	Rate (Hz)
LVL1	μ ($p_T > 6$ GeV, $\vert\eta\vert < 2.4$) triggered by the Muon System	23000
LVL2	LVL1 output spectra convolved with reconstruction efficiency in Inner Detector with cut $p_T > 5.9$ GeV	9000 (2300 $b \to \mu$ 1100 $c \to \mu$ 5400 $K/\pi \to \mu$)

Table 11-18 Summary of *B*-physics triggers: rates of events satisfying the LVL2 trigger selections applied to events already containing one muon with p_T threshold 6 GeV identified at LVL1 and confirmed at LVL2.

	Trigger requirements	Selected *B*-channels	Rate (Hz)
Hadron channels	$D_s \to \phi(K^+K^-)\pi$, 3 hadrons $p_T > 1.5$ GeV, loose mass cuts	$B_s \to D_s \pi$, $B_s \to D_s a_1$	190
	2 hadrons $p_T > 4$ GeV, loose mass, angle and Σp_T cuts	$B_d \to \pi\pi$	80
Electron channels	*ee* pair, $p_T > 0.5$ GeV, identification by TRT, 2.0 GeV < m(*ee*) < 3.8 GeV	$b\bar{b} \to \mu B_d(J/\psi(ee)K^0)$	310
	single *e*, $p_T > 5$ GeV, identification in TRT+ECAL of electron reconstructed with $p_T > 4$ GeV in the Inner Detector	$b\bar{b} \to e\, B_d(J/\psi(\mu\mu)K^0)$	93 [51 from true electrons, 42 from wrongly-identified hadrons]
Muon channels	second μ ($p_T > 5$ GeV, $\vert\eta\vert < 2.5$) identification in muon chambers + matching with the Inner Detector	$B_d \to J/\psi(\mu\mu)(K/K^*)$, $B_s \to J/\psi(\mu\mu)\phi$, $B \to \mu\,\mu$, $B \to K^{0*}\mu\mu$, *etc.*, $\Lambda_b \to \Lambda^0 J/\psi(\mu\mu)$, $B_c \to J/\psi(\mu\mu)\,\pi$	170 [80 from *b/c*, 90 from K/π]
Total LVL2 *B*-physics trigger rate			840 Hz

The results presented in this section for the various *B*-physics trigger channels demonstrate that the total *B*-physics rate from LVL2 can be reduced to ~900 Hz (Table 11-18); this is acceptable for input to the Event Filter. The uncertainties in the rates are due mainly to model-dependence in the prediction of cross-sections, which could be as large as a factor four.

11.7 LVL1 and LVL2 global decision

11.7.1 Introduction

This section presents a set of trigger menus that covers the vast majority of main-stream discovery physics; more details are presented in Refs. [11-1] and [11-27]. The menus are split into two groups, a very simple set of menus covering the majority of main-stream discovery physics, and more specialised triggers. The latter are needed to cover standard physics such as jet cross-section measurements and background studies. They also include monitoring and calibration triggers to read out data relating to the trigger and detector subsystems for technical studies. The trigger menus eventually used by ATLAS will be more complex and will include triggers that are not required for any specific physics analysis. Some of these are covered in the second set of menus. The specialised triggers are those that are needed to understand thresholds, pile-up and to take data for studies of known physics processes. They will make use of a range of prescale factors to limit the rate.

11.7.1.1 Rates

The physics-oriented trigger menus are determined by the best compromise between efficiency for physics channels and affordable trigger rate. The LVL1 trigger rate is dominated by background physics processes such as jet events faking isolated $e/\gamma/\tau$, as well as giving high-p_T jet triggers, and muons from $b/c \to \mu X$, $\pi/K \to \mu\nu$.

The output target rate for LVL1 is ~40 kHz, which allows a safety factor of almost two, compared to the initial design capability of 75 kHz. The estimated uncertainty on the pp inelastic cross-section is about 30%.The total uncertainty on the main background processes, however, could be as large as a factor of two (inclusive jet production at low p_T) to five ($b, c \to \mu$ events). No *K*-factor correction has been used. Corrections for biases resulting from η and p_T (hard scatter) cuts applied for reasons of CPU efficiency in the Monte Carlo simulations, are also only approximate. More details on the cross-sections and simulation tools can be found in [11-1] Chapters 2 and 4, respectively.

The output target rate for LVL2 is around 1 to 2 kHz, but it depends on the optimum separation between LVL2 and the Event Filter, which will not be determined for some time. The majority of LVL2 muon triggers will be genuine prompt muons, whereas the LVL2 isolated e/γ rate is still dominated by jet events. The expected rates for inclusive $W \to e\nu$ and $Z \to ee$ production with $p_T(e) > 30$ GeV are about 50 Hz and 5 Hz, respectively, at high luminosity (10^{34} cm^{-2}s^{-1}). Detailed references and comments for the quoted rates are available in Chapter 11 of [11-1].

11.7.2 Key to the menus

Figure 11-41 summarises the notation used to formulate the trigger menus and define the trigger objects at the various levels. The notation of Tables 11-1 and 11-2 is used to describe the object type.

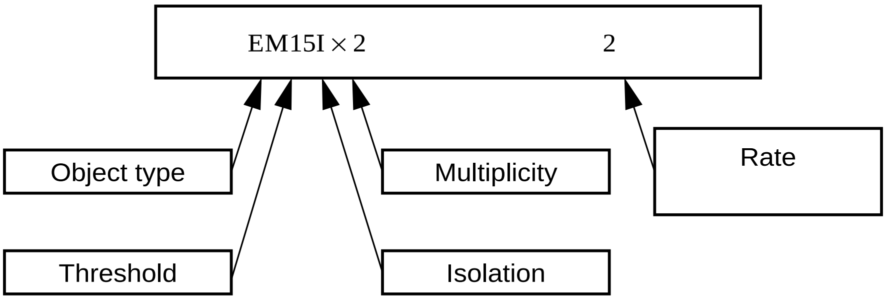

Figure 11-41 Notation used in the menus.

LVL1 trigger objects are shown in capital letters, whereas LVL2 trigger objects start with lower case letters. The E_T threshold and the requirement of isolation are indicated after the object code. The thresholds are generally given at the point where the LVL1 (LVL2) algorithms are 95% (90%) efficient. Exceptions include the E_T^{miss} trigger, where the actual cut is given, and the muon triggers which are given at ~90% efficiency for LVL1. The muon triggers have an additional inefficiency due to the geometric detector acceptance, which is approximately 90%, averaged over the fiducial η coverage.

The isolation thresholds will change with the p_T of the trigger object, becoming looser for higher p_T candidates and being completely removed at very high p_T. At LVL2 the trigger objects may be constrained by additional requirements, like mass cuts. As shown in Table 11-21, more complex objects are used at LVL2 for *B*-physics triggers.

11.7.3 Physics menus

The first set of menus covers the majority of LHC physics studies. They are intended to provide a common focus for physics and trigger-performance studies. They are designed to be simple, inclusive and to satisfy the physics requirements with as short a list of trigger items as possible. The one exception to this is *B*-physics, where selection of particular decay modes must be done in the LVL2 trigger. Where isolation of objects is indicated, it should be understood that the isolation criteria are relaxed as object E_T and multiplicity increase. For very high E_T, isolation is not required. No use is made of veto conditions, though they may be applied at LVL1 and LVL2.

11.7.3.1 LVL1 low luminosity

The LVL1 menu for low luminosity is shown in Table 11-19. The MU6 trigger selects events for *B*-physics studies. The threshold for the two EM object trigger is set as low as possible to maximise the efficiency for $H \to \gamma\gamma$ and $Z \to ee$ decays. If possible the threshold will be lowered further to give some acceptance for high-p_T J/ψ and Υ decays to *ee*.

The inclusive-jet threshold has been set high to reduce the rate and make more room for other triggers. This is because the additional jet rejection available at LVL2 is small, so the useful LVL1 threshold is effectively limited by LVL2 rate requirements. Multi-jet and jet+E_T^{miss} triggers are given priority when sharing out the rate budget for these types of triggers. The thresholds of the multi-jet triggers are also chosen to give acceptable rates for LVL2. No specific requirements from the physics have been stated which would dictate specific values for these thresholds.

For the J50 + XE50 and T20 + XE30 triggers [11-14], the thresholds and rates should be taken as indicative. These triggers are intended to provide efficient inclusive triggers for SUSY production, and also for calibration via $W \rightarrow \tau\nu$ / $Z \rightarrow \tau\tau$. The additional requirement of missing energy allows lower thresholds than are possible with the jet and τ/hadron inclusive triggers. The aim for these triggers is a missing-E_T threshold of around 30–50 GeV and the lowest possible jet and τ thresholds that give an acceptable rate at both LVL1 and LVL2. It should be noted that there is no direct physics need for the LVL1 τ trigger.

The table entry 'Other triggers' indicates the rate budget which is reserved for specialised, monitoring and calibration triggers that are described later in this document.

Table 11-19 LVL1 low and high-luminosity menus.

Low luminosity		High luminosity	
Trigger	**Rate (kHz)**	**Trigger**	**Rate (kHz)**
MU6	23	MU20	3.9
		MU6 × 2	1
EM20I	11	EM30I	22
EM15I × 2	2	EM20I × 2	5
J180	0.2	J290	0.2
J75 × 3	0.2	J130 × 3	0.2
J55 × 4	0.2	J90 × 4	0.2
J50 + XE50	0.4	J100 + XE100	0.5
T20 + XE30	2	T60 + XE60	1
		MU10 + EM15I	0.4
Other triggers	5	Other triggers	5
Total	**44**	**Total**	**40**

11.7.3.2 LVL1 high luminosity

The LVL1 high-luminosity menu in Table 11-19 contains mostly the same objects as the low luminosity menu, but with higher thresholds and/or rates. An additional trigger at high luminosity is MU10 + EM15I. Another extra trigger EM20I + XE is being studied. The additional physics that might be caught by these triggers at high luminosity is *e.g.* $W \rightarrow e\nu$ and $Z \rightarrow \tau\tau$ for calibration purposes.

11.7.3.3 LVL2 low luminosity

Most of the menu items in the low-luminosity LVL2 trigger menu, Table 11-20, follow directly from the LVL1 items in Table 11-19. EM triggers can be refined at LVL2 into candidates for electrons and/or photons. It is possible to apply isolation criteria to the muon triggers to help reduce the rate. Events that satisfy the MU6 LVL1 trigger and the LVL2 μ6 preselection are passed to the *B*-physics menu, described in the next section. The inclusive single-muon trigger μ20 does not require isolation. An inclusive di-muon trigger μ6 + μ5 can be found in the *B*-physics menu (Table 11-21). The trigger μ6i + e15i is an example of the use of a secondary RoI (in this case EM15I) which would not in itself constitute a LVL1 trigger.

Table 11-20 LVL2 low- and high-luminosity menus.

Low luminosity		High Luminosity	
Trigger	**Rate (Hz)**	**Trigger**	**Rate (Hz)**
μ20	200	μ20i	200
		$\mu 6 \times 2 + m_B$	10
		$\mu 10 \times 2$	80
e20i	100	e30i	600
e15i × 2	~few Hz	e20i × 2	20
γ40i	100	γ60i	400
γ20i × 2	5	γ20i × 2	100
j180	100	j290	120
j75 × 3	80	j130 × 3	80
j55 × 4	40	j90 × 4	80
j50 + xE50	250	j100 + xE100	~few 100
τ20 + xE30	400	τ60 + xE60	~few 100
μ6i + e15i	15	μ10i + e15i	20
B-physics	1150		
Other triggers	100	Other triggers	100
Total	**2400**	**Total**	**2000**

As at LVL1, the additional requirement of missing energy in the SUSY/calibration triggers (j50 + xE50, τ20 + xE30), allows lower thresholds than for the inclusive triggers. It is not necessarily expected that xE will be recalculated at LVL2, but the LVL1 E_T^{miss} value could be refined, for example by including muon E_T and correcting for LVL1 calorimeter trigger ADC saturation. For the rates given here, no LVL2 refinement has been taken into account.

11.7.3.4 LVL2 low luminosity *B*-physics

The low-luminosity *B*-physics trigger menu will only be used if the LVL1 trigger includes a MU6 object, and the LVL2 trigger confirms a μ6 trigger.

Table 11-21 Example of *B*-physics trigger menu.

Trigger Signature	Rate (Hz)	Example Channel
μ6 + additional μ5	170	Inclusive $J/\psi \to \mu^+\mu^-$
μ6 + e0.5 × 2 + m_{ee}	310	$b \to \mu X$, $B \to J/\psi\ X \to ee$
μ6 + e5	100	$b \to eX$, $B \to J/\psi\ X \to \mu\mu$ (second μ not required in trigger)
μ6 + h5 × 2 + m_B	80	$b \to \mu X$, $B_d \to \pi^+\pi^-$
μ6 + h1.5 × 3 + m_ϕ + m_{Ds}	190	$b \to \mu X$, $B_s \to D_s(\phi^0(K^+K^-)\pi)X$
μ6 + ...	300	reserved for additional *B* channels
Total	**1150**	

The rates after the LVL2 selection are given in Table 11-21. There is little overlap between the trigger items so the total rate is approximately equal to the sum of the rates for the individual triggers.

11.7.3.5 LVL2 high luminosity

Most menu items in the LVL2 high-luminosity menu, Table 11-20, follow directly from the LVL1 items of Table 11-19. Compared to low luminosity, thresholds have generally been raised and the requirement of isolation has been added to the inclusive muon trigger. The di-muon triggers without isolation requirements are useful for *B*-physics. The rate for the di-electron trigger e20i × 2 is almost a complete subset of γ20i × 2, so the rate is not included in the total.

11.7.4 Menus for specialised triggers

Redundant triggers are needed for cross checks. Inclusive triggers are prescaled with lower thresholds to understand threshold behaviour, collect background samples, and to take low-p_T data. The rates will be controlled by choices of threshold and prescale factors. The rate budgets include 5 kHz at LVL1 and 100 Hz at LVL2 for these triggers. At this stage, the most important aspect is to know the number of thresholds required as this has implications for the design of the LVL1 trigger.

A number of additional inclusive triggers, with high thresholds and low rates without prescaling are foreseen: τ / hadron; E_T^{miss}; $\sum E_T$, $\sum E_T^{jet}$. A localised forward-energy trigger is also under consideration.

Prescaled triggers are foreseen with a range of thresholds. Typically, these would have four to six (possibly low) thresholds per trigger, each with a different prescale factor. Prescaled triggers will include: single jet, three jets, four jets; muon, di-muon; electron / photon; τ / hadron; E_T^{miss}; $\sum E_T$, $\sum E_T^{jet}$; forward-energy (under consideration).

In addition to the specialised physics triggers listed above, some more technical triggers are foreseen. These include detector-calibration triggers, as well as a random trigger and a trigger on bunch crossings, including a trigger on empty bunch crossings.

11.7.5 Physics coverage of the trigger menus

It is believed that the set of triggers proposed in Tables 11-19 and 11-20 covers most of the physics goals of the experiment. In fact, many processes will be selected through multiple trigger signatures, thus providing optimal efficiency and several means of measuring the trigger efficiency.

Inclusive lepton and di-lepton triggers provide $W \to l\nu$ and $Z \to ll$ selections, where l designates an electron or a muon. They therefore give an unbiased trigger for many Standard Model physics processes and also for many searches for physics beyond the Standard Model. At low luminosity, $W \to l\nu$ and $Z \to ll$ decays are selected by the MU6 / EM20I LVL1 triggers and the μ20 / e20i LVL2 triggers; $Z \to ll$ decays are also selected by the EM15I × 2 LVL1 triggers and the μ6 + μ5 / e15i × 2 LVL2 triggers.

At high luminosity, the $W \to l\nu$ decays can still be selected by inclusive lepton triggers, although with a somewhat high threshold in the case of electrons (MU20 / EM30I at LVL1 and μ20i / e30i at LVL2). A trigger on an isolated electron with a lower threshold and an additional E_T^{miss} requirement is being studied at high luminosity in LVL1 and LVL2 in order to recover efficiency for the inclusive $W \to l\nu$ selection. In contrast the thresholds for the inclusive $Z \to ll$ decays remain comfortably low (MU6 × 2 / EM20I × 2 at LVL1 and μ10 × 2 / e20i × 2 at LVL2).

As mentioned above, many physics processes of interest are covered by the inclusive lepton / di-lepton triggers. Examples include the following.

- Gauge-boson pair production, for the study of anomalous couplings and to investigate the behaviour of the production cross-section at high mass.
- Top-quark production (single top or $t\bar{t}$ pairs), for all cases except $t\bar{t}$ production with fully-hadronic top decays.
- Direct production of SM or MSSM Higgs bosons with $H \to ZZ^{(*)}$, $WW^{(*)}$ decays, over the full Higgs mass range of interest. Associated production of SM Higgs bosons through $WH/ZH/t\bar{t}H$ processes, with $H \to b\bar{b}$ or $H \to \gamma\gamma$, and $W \to l\nu$ or $Z \to ll$.
- Decays of MSSM Higgs bosons, such as $A \to Zh$, $H/A \to \mu\mu$, $H/A \to t\bar{t}$, and also $H/A \to \tau\tau$ with one leptonic τ decay. Production of $t\bar{t}$ with one top decay to bH, where the other top-quark decay provides the inclusive W trigger.
- Production of new vector gauge bosons (W'/Z'), with W'/Z' decays to leptons. Also, resonance production at the TeV scale (strongly interacting Higgs sector), with resonance decays into gauge-boson pairs.
- Production of supersymmetric particles with final states containing: at least one high-p_T lepton and large E_T^{miss} in the case of R-parity conservation; or at least one high-p_T lepton (*e.g.* from $\chi_2^0 \to ll\chi_1^0$ decay) with or without large E_T^{miss} in the case of R-parity violation with $\chi_1^0 \to 3$ jets, $\chi_1^0 \to l\nu\nu$, or $\chi_1^0 \to ll'\nu$.
- Searches for leptoquarks decaying into electrons or muons; searches for compositeness in the lepton sector through Drell-Yan production.

The remaining physics channels not covered by the inclusive lepton / di-lepton (and electron + E_T^{miss}) triggers discussed above are:

- *B*-physics, which is covered in a separate menu in Table 11-21. A budget has been foreseen at LVL2 for B decay channels that are not yet part of the studies.

- $H \to \gamma\gamma$ decays from direct Higgs production, which are covered by EM15I × 2 (EM20I × 2) for LVL1 and by γ20i × 2 (γ20i × 2) for LVL2 at low (high) luminosity. These triggers also cover possible MSSM Higgs boson decays such as $H \to hh \to b\bar{b}\gamma\gamma$.
- Searches for supersymmetry involving high-p_T jets with or without E_T^{miss}. At low luminosity the combination of J50 + xE50, J180, and J75 × 3 / J55 × 4 triggers provides excellent coverage for all exclusive final states of interest not containing leptons. In the case of R-parity conservation, final states containing at least two high-p_T jets and large E_T^{miss} (typically two jets with E_T > 150 GeV and E_T^{miss} > 200 GeV) provide a broad inclusive sample for more exclusive searches. In the case of R-parity violation, with χ_1^0 decaying predominantly to three jets. Here the multi-jet triggers will cover most of the exclusive final states of interest. To date the only exclusive final states which have been proven to be observable above the huge potential QCD background are those containing isolated high-p_T leptons.

  At high luminosity, the higher thresholds applied to the various jet triggers and to the jet+E_T^{miss} trigger will be well suited to searches for higher-mass SUSY particles.
- Searches for leptoquarks decaying into a jet and a neutrino that rely on the jet+E_T^{miss} trigger.
- Searches for resonances decaying into jets and for compositeness in the quark structure. These rely largely on the inclusive single-jet trigger (*e.g.* additional vector bosons or technicolour resonances decaying to two jets) or on multi-jet triggers (*e.g.* purely hadronic decays of $t\bar{t}$ pairs), both at low and high luminosity.

A τ+E_T^{miss} trigger may increase the sensitivity to specific SUSY signatures for high values of tan β. It is also expected that the large variety of fairly inclusive triggers presented here would be sensitive to other new physics.

Finally, it is important to emphasise that much of the early large cross-section physics (*e.g.* QCD jets, direct photons, *etc.*) will be studied using more inclusive triggers than the ones quoted explicitly in the menus of Tables 11-19 and 11-20.

11.8 The task of the Event Filter

The task of the Event Filter (EF) is to make the final selection of physics events which will be written to mass storage for subsequent full offline analysis, and to reduce the trigger rates to as close to the real physics rates as possible. This should allow one to reduce the output data rate from LVL2 by an order of magnitude, giving ~100 Hz if the full event data are to be recorded. Event-summary information could be recorded at much higher rates, possibly for certain specific triggers (*e.g.* single-jet or multi-jet triggers for high-statistics QCD studies involving only the calorimeter information) but certainly not for the main-stream trigger items, which make up the bulk of the LVL2 selected events.

After event building, the EF will be able to perform detailed reconstruction using the complex algorithms of the offline code itself. All event data are accessible at the EF level for calculations and selections, though only part of these data will be used by the algorithms. Similar to the LVL2 guidance by LVL1, the EF algorithms will be guided by the LVL2 results and possibly by the LVL1 secondary-RoI information. The processing by the EF must result in efficient and complete tagging of the events to prepare efficient event selection for physics analysis. Depending on the processing time needed by the algorithms, the processing power available, and the stability of the calibrations and beam position, one may aim at completing in the EF the reconstruction to such a degree that the subsequent analysis steps have only to perform hypothesis-dependent updates of the reconstruction. Thanks to this potential performance, cut adjustments which are not possible at LVL2 will become possible; the exact selection criteria to be used have not yet been chosen.

In contrast to LVL1 and LVL2, some of the EF output rates expected are of the same order of magnitude as the signal itself, as shown below in a few cases for low and high-luminosity operation. Many processes will be selected through multiple trigger signatures, thus providing optimal efficiency and several means of controlling the crucial aspects of the trigger efficiency. Inclusive lepton and di-lepton triggers provide $W \to l\nu$ and $Z \to ll$ selections. They therefore give an unbiased trigger for many Standard Model physics processes and also for many searches for physics beyond the Standard Model, as discussed in the previous section.

The most challenging of these inclusive $W \to l\nu$ or $Z \to ll$ triggers is certainly the $W \to e\nu$ trigger, which has an expected output rate from LVL2 of 600 Hz at high luminosity for $p_T^e > 30$ GeV. Most of this output rate is still due to background from charged hadrons and from photon conversions (see Section 11.4.3). On the other hand, the expected rate for the inclusive $W \to e\nu$ signal events with $p_T^e > 30$ GeV and an additional cut requiring $E_T^{miss} > 25$ GeV is of order 50 Hz.

The above numbers clearly show that one of the main tasks of the EF will be to bring the rate of inclusive $W \to e\nu$ trigger candidates as close as possible to the real physics rate through a combination of tighter electron-identification cuts and of loose E_T^{miss} cuts. Whether the total expected rate of ~50 Hz would be acceptable or not is a matter for further study. More exclusive processes containing $W \to e\nu$ decays are, however, expected to have much lower trigger rates after the Event Filter. For example, the rate for signal events containing a $W \to e\nu$ decay and two jets with $E_T > 30$ GeV and within $|\eta| < 2.5$ is expected to be below a few Hz. This shows that the EF can provide a moderate output rate for all physics searches of the type $WH / ZH / t\bar{t}H$ production with $H \to b\bar{b}$ and $W \to l\nu$ / $Z \to ll$, possibly without processing the event further in the Inner Detector, and without improving the electron identification, which was provided by LVL2. The rate for signal events from top-quark production containing at least one high-p_T electron (or muon) is expected to be of the order of 1 Hz at high luminosity. Again, these events can be selected by the EF in a very inclusive way.

Obviously, the task of the EF in terms of selecting inclusive $W \to \mu\nu$ decays or $Z \to ll$ decays is easier than that of selecting inclusive $W \to e\nu$ decays. This is because the expected LVL2 output rates for the high-p_T single muon trigger and for the isolated high-p_T di-lepton triggers are much lower than for the high-p_T single isolated electron trigger. The expected rate for inclusive $Z \to ll$ signal events is 10 Hz at high luminosity, and the EF will clearly be able to approach that rate by using *e.g.* a mass cut on the lepton pair.

The physics channels not covered by the inclusive lepton / di-lepton (and electron+E_T^{miss}) triggers were listed in the previous section. The area of *B*-physics is another challenging task for the Event Filter, since the expected output rate from LVL2 is of the order of 1 kHz for *B*-physics alone at low luminosity and since most of the candidate events are genuine *B*-events. A complete and accurate reconstruction of the Inner Detector information is necessary in order to further reduce the rate, for example using vertexing cuts. The largest rate from physics channels to be analysed in this field is for inclusive $J/\psi \to \mu\mu$ decays with $p_T^{\mu_1} > 6$ GeV and $p_T^{\mu_2} > 5$ GeV. The total expected rate for signal events is about 5 Hz from direct J/ψ production and about 3 Hz from inclusive $B \to J/\psi$ production. These events are expected to be heavily used in *CP*-violation studies with jet-charge and B–π tagging methods applied in addition to the more traditional lepton tagging. To reduce the LVL2 output rates to values close to the physics rates quoted above, a combination of vertexing cuts on the muon pair and of tighter kinematic cuts, including mass cuts, will have to be performed by the Event Filter. The more exclusive *B*-decays are expected to contribute at much lower levels of typically 0.1 Hz per channel or less.

It is also hoped that the large variety of fairly inclusive triggers presented here would be sensitive to unexpected new physics. Finally, it is important to emphasise that much of the early large cross-section physics (*e.g.* QCD jets, direct photons, *etc.*) will be studied using more inclusive triggers than the ones quoted explicitly in Section 11.7 as well as dedicated algorithms in the Event Filter.

The menus and rates presented in Section 11.7 will be used as basis for menus for more detailed studies of both the LVL2 trigger and the Event Filter, in terms of performance and of implementation. Those trigger items that are considered particularly challenging or critical will be subject to detailed trigger performance studies using fully-simulated data as input and offline reconstruction code as a reference. Wherever possible, the trigger-performance results will be parametrised for use in fast simulations with high-statistics background samples. A complete set of output rates for the EF can only be obtained through a combination of detailed full-simulation studies and of fast-simulation studies, which use parametrised detector performance.

In conclusion, the role of the Event Filter will be very important in determining the scope and breadth of physics channels available to ATLAS to study in detail the physics channels of interest and to constrain as well as possible the background estimates to possible new physics. It is hoped that most of the physics goals, with the notable exception of *B*-physics, can be achieved with RoI-guided processing, *i.e.* avoiding complete processing of the Inner Detector information.

11.9 References

11-1 ATLAS Collaboration, Trigger Performance Status Report, CERN / LHCC 98-15 (1998).

11-2 ATLAS Collaboration, First-Level Trigger Technical Design Report, ATLAS TDR 12, CERN / LHCC / 98-14 (1998).

11-3 ATLAS Collaboration, Technical Proposal, CERN / LHCC / 94-43 (1994).

11-4 ATLAS Collaboration, DAQ, EF, LVL2 and DCS Technical Progress Report, CERN / LHCC / 98-16 (1998).

11-5 Level-1 muon trigger group, ‘Improvements to the level-1 muon trigger giving increased robustness against backgrounds’, ATLAS Communication ATL-COM-DAQ-99-011 (1999).

11-6 P. Eerola, ‘The inclusive muon cross-section in ATLAS’, ATLAS Internal Note ATL-MUON-98-222 (1998).

11-7 T. Sjostrand, ‘PYTHIA 5.7 and JETSET 7.4 Physics and Manual’, CERN-TH.7112 / 93 (1993).

11-8 J. Ranft, ‘*DPMJET* version II.3 and II.4: sampling of hadron–hadron, hadron–nucleus and nucleus–nucleus interactions at cosmic-ray energies, according to the Dual Parton Model’, INFN-AE-97-45 (1997).

11-9 A.I. Drozhdin *et al.*, Nucl. Instrum. Methods **A381** (1996) 531.

11-10 S. Robins, ‘Level-1 trigger rate from beam-halo muons in the end-cap’, ATLAS Internal Note ATL-DAQ-98-128 (1998).

11-11 A. Ferrari *et al.*, Z. Phys. **C70** (1996) 413, and FLUKA manual http://www.cern.ch/alice/Projects/offline/Simulation/fluka

11-12 D. Costanzo *et al.*, 'Muon trigger with TileCal, a preliminary investigation', ATLAS Internal Note ATL-DAQ-99-002 (1999).

11-13 S. Catani *et al.*, Nucl. Phys. **B406** (1993) 187.

11-14 R. Dubitzky *et al.*, 'Level-1 rates for triggers using the missing-E_T signature', ATLAS Internal Note ATL-DAQ-98-011 (1998).

11-15 N. Baytch *et al.*, 'A method for a LVL2 muon trigger for ATLAS', ATLAS Internal Note ATL-DAQ-99-003 (1999).

11-16 T.G. Shears, 'Studies of muon isolation in the level-2 muon trigger', ATLAS Internal Note ATL-DAQ-98-122 (1998).

11-17 S. Gonzalez, T. Hansl-Kozanecka and M. Wielers, 'Selection of high-p_T electromagnetic clusters by the Second Level trigger of ATLAS', ATLAS Communication ATL-COM-DAQ-99-009 (1999).

11-18 J. Baines *et al.*, 'Identification of high-p_T electrons by the Second Level Trigger of ATLAS', ATLAS Communication ATL-COM-DAQ-99-007 (1999).

11-19 M. Wielers, 'Photon Identification with the ATLAS Detector', ATLAS Communication ATL-COM-PHYS-99-011 (1999).

11-20 J. Baines, R. Dankers and S. Sivoklokov, 'Performance of a LVL2 trigger feature-extraction algorithm for the Precision Tracker', ATLAS Communication ATL-COM-DAQ-99-008 (1999).

11-21 ATLAS Collaboration, Inner Detector Technical Design Report, ATLAS TDR 4, CERN/LHCC/97-16 (1997).

11-22 E. Richter-Was and D. Froidevaux, 'MSSM Higgs searches in multi-*b*-jet final states', ATLAS Internal Note ATL-PHYS-97-104 (1997).

11-23 J. Baines *et al.*, 'Global Pattern Recognition in the TRT for *B*-Physics in the ATLAS Trigger', ATLAS Communication ATL-COM-DAQ-99-004 (1999).

11-24 R.E. Kalman, Trans. ASME, J. Basic Eng. **82D** (1960) 35.

11-25 I. Gavrilenko, 'Description of global pattern-recognition program (xKalman)', ATLAS Internal Note ATL-INDET-97-165 (1997).

11-26 S. Sivoklokov, 'TRT Trigger performance in the solenoidal magnetic field', ATLAS Communication ATL-COM-DAQ-99-005 (1999).

11-27 S. George and T. Hansl–Kozanecka (eds), 'ATLAS Trigger Menus', ATLAS Internal Note ATL-DAQ-98-121 (1998).

11-28 E. Richter-Was, D. Froidevaux and L. Poggioli, 'ATLFAST 1.0 A package for particle-level analysis', ATLAS Internal Notes ATL-PHYS-96-079 (1996) and ATL-PHYS-98-131 (1998).